Dysregulated Generation of Follicular Helper T Cells in the Spleen Triggers Fatal Autoimmune Hepatitis in Mice

NOBUHIRO AOKI,[*,‡] MASAHIRO KIDO,[*,‡] SATORU IWAMOTO,[*,‡] HISAYO NISHIURA,[*,‡] RYUTARO MARUOKA,[*,‡] JUNYA TANAKA,[*,‡] TAKESHI WATANABE,[*] YOSHIMASA TANAKA,[*] TAKU OKAZAKI,[§] TSUTOMU CHIBA,[‡] and NORIHIKO WATANABE[*,‡]

*Center for Innovation in Immunoregulative Technology and Therapeutics and ‡Department of Gastroenterology and Hepatology, Graduate School of Medicine, Kyoto University, Kyoto; and §Division of Immune Regulation, Institute for Genome Research, University of Tokushima, Tokushima, Japan

BACKGROUND & AIMS: To clarify mechanisms involved in the development of autoimmune hepatitis (AIH), we recently developed a mouse model of spontaneous AIH by inducing a concurrent loss of Foxp3+ regulatory T cells and programmed cell death 1 (PD-1)–mediated signaling. Fatal AIH in these mice was characterized by severe T-cell infiltration and huge production of antinuclear antibodies (Abs). This study aims to identify induction sites, responsible T-cell subsets, and key molecules for induction of AIH. **METHODS:** To develop the mouse model of AIH, neonatal thymectomy (NTx) was performed on PD-1–deficient (PD-1$^{-/-}$) mice. We then conducted neonatal splenectomy or in vivo administration of Abs to cytokines, chemokines, or cell-surface molecules. **RESULTS:** In NTx-PD-1$^{-/-}$ mice, either neonatal splenectomy or in vivo CD4+ T-cell depletion suppressed CD4+ and CD8+ T-cell infiltration in the liver. In the induction phase of AIH, splenic CD4+ T cells were localized in B-cell follicles with huge germinal centers and showed the Bcl6+ inducible costimulator (ICOS)+ interleukin (IL)-21+ IL-21 receptor (IL-21R)+ follicular helper T (T$_{FH}$) cell phenotype. Blocking Abs to ICOS or IL-21 suppressed T$_{FH}$-cell generation and induction of AIH. In addition, IL-21 produced by T$_{FH}$ cells drove CD8+ T-cell activation. Splenic T$_{FH}$ cells and CD8+ T cells expressed CCR6, and CCL20 expression was elevated in the liver. Administration of anti-CCL20 suppressed migration of these T cells to the liver and induction of AIH. **CONCLUSIONS:** Dysregulated T$_{FH}$ cells in the spleen are responsible for the induction of fatal AIH, and CCR6-CCL20 axis-dependent migration of splenic T cells is crucial to induce AIH in NTx-PD-1$^{-/-}$ mice.

Keywords: Autoimmune Liver Disease; Pathogenesis; Follicular Helper T Cells.

H uman autoimmune hepatitis (AIH) shows varied clinical manifestations ranging from asymptomatic, mild chronic hepatitis to acute-onset fulminant hepatic failure. The histologic findings of AIH are characterized by a mononuclear cell infiltration invading the parenchyma, ranging from piecemeal necrosis to submassive lobular necrosis.[1,2] The serologic hallmark of AIH is the production of a variety of characteristic circulating autoantibodies (autoAbs), including anti-nuclear Abs (ANAs).[1,2] Although AIH appears to be a T cell-mediated autoimmune disease, it is unclear which type of effector T cells are involved and how the dysregulated T cells trigger the development of AIH.

Recently, we developed the first mouse model of spontaneous fatal AIH resembling acute-onset AIH presenting as fulminant hepatic failure in humans.[3] Neither programmed cell death 1 (PD-1)–deficient mice (PD-1$^{-/-}$ mice) nor BALB/c mice thymectomized 3 days after birth (NTx mice), which severely reduces the number of naturally arising Foxp3+ regulatory T cells (Tregs) in periphery, developed inflammation of the liver. However, PD-1$^{-/-}$ BALB/c mice with neonatal thymectomy (NTx-PD-1$^{-/-}$ mice) developed fatal AIH, suggesting that immune dysregulation by a concurrent loss of naturally arising Tregs and PD-1–mediated signaling can induce fatal AIH. Because of the massive destruction of the parenchyma of the liver, these mice started to die as early as 2 weeks of age, with most dying by 4 weeks. In humans, liver tissue injury in AIH is mediated not only by CD4+ but also by CD8+ T cells.[4,5] Especially in acute-onset human AIH, activated CD8+ T cells are thought to play a crucial role in the pathogenesis.[6] Fatal AIH in NTx-PD-1$^{-/-}$ mice was characterized by CD4+ and CD8+ T-cell infiltration with massive lobular necrosis and huge ANA production; activated CD8+ T cells were mainly involved in progression to fatal hepatic damage.[3] We showed that the infiltrated CD4+ and CD8+ T cells in the severely damaged liver produced large amounts of inflammatory cytokines, such

as interferon (IFN)-γ and tumor necrosis factor-α. However, it is unclear whether these effector T cells are also crucial in the induction phase of the disease.

Follicular helper T (T$_{FH}$) cells are a newly defined effector T cell subset that provides powerful help to B cells in forming germinal centers (GCs).[7-9] T$_{FH}$ cells arise from activated T cells that express Bcl6, a master transcription factor for T$_{FH}$-cell differentiation.[8,9] Differentiated T$_{FH}$ cells express interleukin (IL)-21, IL-21 receptor (IL-21R), inducible costimulator (ICOS), CXC chemokine receptor (CXCR)5, and PD-1. IL-21 and ICOS are indispensable for T$_{FH}$-cell generation and helper function to B cells.[7-9] CXCR5 promotes the colocalization of T$_{FH}$ cells and B cells in GCs.[7-9] Although CXCR5$^+$ T$_{FH}$ cells are localized mainly in the GC$^+$ B-cell follicles, a recent study showed that circulating T cells resembling T$_{FH}$ cells existed in the peripheral blood of patients with B cell–mediated autoimmunity.[10] In addition, IL-21 has the potential to modulate the activity of CD8$^+$ T cells and other immune and nonimmune cells in vivo.[11] Although AIH appears to be a T cell–mediated autoimmune disease, it is characterized by hyper-γ-globulinemia and the production of a variety of circulating autoAbs, suggesting that B-cell activation including B cell–mediated autoimmunity is associated with its development. Thus, it may be possible that dysregulated T$_{FH}$ cells are involved in both T cell- and B cell–mediated autoimmunity in AIH.

In this study, using our new mouse model of AIH, we examined the T-cell subsets responsible for induction of AIH and the mechanisms by which these T cells initiate fatal AIH. We found that splenic CD4$^+$ T cells are responsible for induction of fatal AIH. In these mice, splenic CD4$^+$ T cells were autonomously differentiated into T$_{FH}$ cells. Moreover, dysregulated T$_{FH}$ cells not only promoted ANA production but also directly migrated into the liver, triggering the induction of fatal AIH.

Materials and Methods

Methods

All protocols for mice, enzyme-linked immunosorbent assay, administration of Abs in vivo, histologic and immunohistologic analysis, flow cytometry analysis and isolation of lymphocytes, adoptive transfer, real-time quantitative reverse-transcription polymerase chain reaction, and T-cell coculture are detailed in Supplementary Methods.

Statistical Analysis

The data are presented as the mean values $\pm$ standard deviations. Statistical analysis was performed by the Student t test for pairwise comparisons. Survival rates were estimated by the Kaplan–Meier method and compared with the log-rank test. P values below .05 were considered significant.

Results

Splenic CD4$^+$ T Cells Are Responsible for Induction of Fatal AIH

Fatal AIH developed in 3-week-old NTx-PD-1$^{-/-}$ mice was characterized by severe CD4$^+$ and CD8$^+$ T-cell infiltration.[3] To examine whether CD4$^+$ and/or CD8$^+$ T cells are indispensable for the development of fatal AIH, NTx-PD-1$^{-/-}$ mice were injected intraperitoneally at 1 day after NTx and then once a week with either anti-CD4 or anti-CD8 monoclonal antibodies (mAbs). After 4 injections of anti-CD4 or anti-CD8, the number of CD4$^+$ or CD8$^+$ T cells in the periphery was greatly reduced, respectively, and fatal AIH was suppressed (Figure 1A and data not shown). Importantly, depletion of CD4$^+$ T cells inhibited the infiltration of CD8$^+$ T cells in the liver, whereas depletion of CD8$^+$ T cells allowed CD4$^+$ T cells to infiltrate (Figure 1B). These data suggest that both CD4$^+$ and CD8$^+$ T cells are indispensable for the development of fatal AIH and that the infiltration of CD8$^+$ T cells in the liver is regulated by CD4$^+$ T cells.

Three-week-old NTx-PD-1$^{-/-}$ mice with severe AIH showed splenomegaly, and the spleen in these mice became enlarged as early as 2 weeks of age (Figure 1C). To determine whether the spleen is an induction site for fatal AIH, we performed neonatal splenectomy in these mice. We found that neonatal splenectomy suppressed mononuclear infiltration as well as destruction of organ structure in the liver, leading to a significantly higher survival rate (Figure 1D and E). We had previously demonstrated that transfer of total but not CD4$^+$ T-cell depleted splenocytes from NTx-PD-1$^{-/-}$ mice into recombination activating gene 2 (RAG2)$^{-/-}$ mice induced the development of severe hepatitis.[3] Taken together, these data suggest that the spleen is an induction site for AIH and that splenic CD4$^+$ T cells are responsible for induction of fatal AIH.

Splenic CD4$^+$ T Cells in NTx-PD-1$^{-/-}$ Mice Are Preferentially Localized Within GC-Bearing B-Cell Follicles

After the spleen became enlarged at 2 weeks of age, hepatic damage from AIH was apparent at 2 to 3 weeks in NTx-PD-1$^{-/-}$ mice.[3] When we looked in situ at the spleen of 2-week-old NTx-PD-1$^{-/-}$ mice, most of the CD4$^+$ T cells were preferentially localized within B220$^+$ B-cell follicles, whereas CD8$^+$ T cells were mainly localized outside the follicles. Interestingly, B-cell follicles with CD4$^+$ T-cell accumulation autonomously developed peanut agglutinin (PNA)$^+$ GCs (Figure 1F, *left lower panels*, and Supplementary Figure 1). Seven days after thymectomy, 1.5-week-old NTx-PD-1$^{-/-}$ mice showed scattered accumulation of CD4$^+$ T cells with B220$^+$ B cells in the spleen (Figure 2A). Diffuse accumulation of CD4$^+$ T cells in the follicles with GC formation developed in the spleen of 2-week-old mice and progressed in
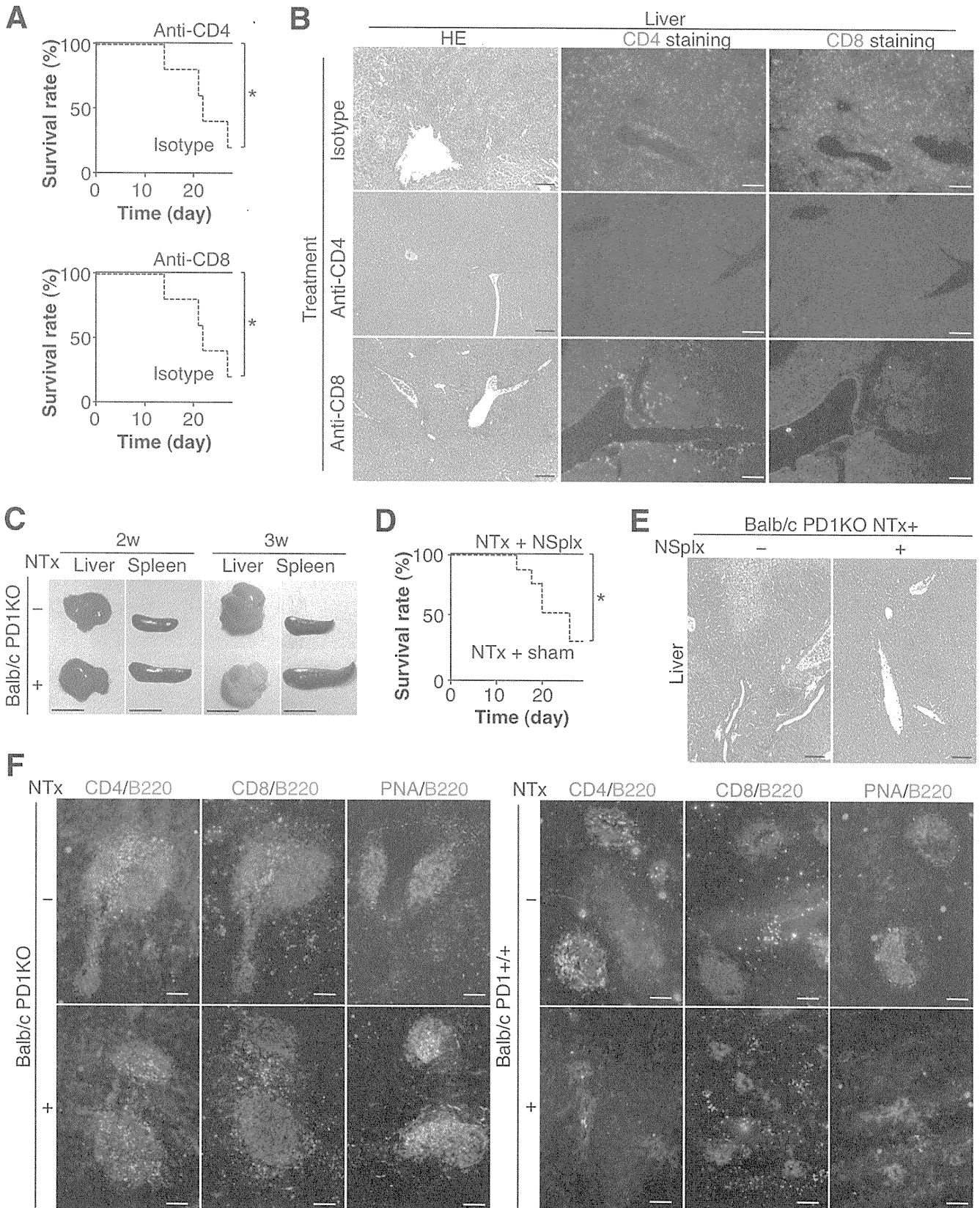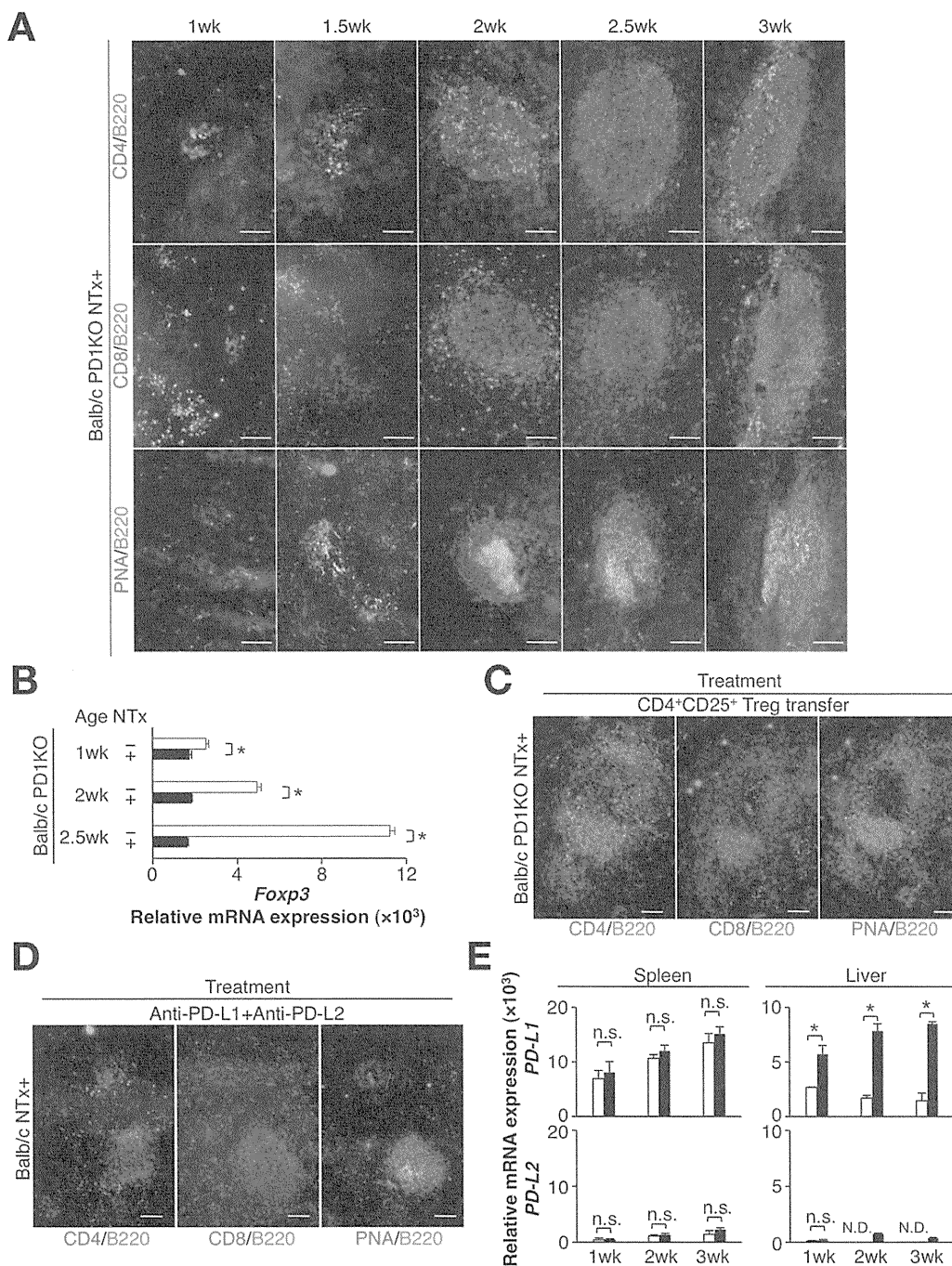
Figure 2. Autonomous localization of splenic CD4⁺ T cells within GC⁺ follicles depends on concurrent loss of naturally arising Tregs and PD-1 mediated signaling. (A) The spleens from indicated mice at 1 to 3 weeks of age were stained as described in Figure 1F. (B) Foxp3 mRNA expression by CD4⁺ T cells from the spleen of indicated mice. (C) Double immunostainings of the spleen from 2-week-old NTx-PD-1⁻/⁻ mice transferred with splenic Tregs from normal BALB/c mice. The spleens were stained as described in Figure 1F. (D) Double immunostainings of the spleen in 2-week-old NTx mice injected at days 3 and 10 with anti-PD-L1 and anti-PD-L2. The spleens were stained as described in Figure 1F. (E) PD-L1 and PD-L2 mRNA expressions of liver and spleen of PD-1⁻/⁻ mice at indicated age in weeks with (solid columns) or without (open columns) NTx. Bars indicate the mean of each group, and short bars indicate the standard deviation. *P < .05. N.D., not detected; n.s., not significant. All scale bars, 100 μm.

Figure 1. Splenic CD4⁺ T cells are responsible for induction of fatal AIH. (A and B) NTx-PD-1⁻/⁻ mice were injected intraperitoneally at 1 day after NTx and then once a week with anti-CD4 (n = 5), anti-CD8 (n = 5), or isotype (n = 5) Abs. After 4 injections, mice at 4 weeks of age were killed, and the livers were harvested. (A) Survival rate of the mice and (B) stainings of the liver for hematoxylin and eosin (HE), CD4, and CD8 at 4 weeks. (C) Macroscopic view of the liver and spleen from indicated mice. (D) Survival rate and (E) histology of the liver from 4-week-old NTx-PD-1⁻/⁻ mice with (n = 7) or without (n = 9) neonatal splenectomy (NSplx). (F) The spleens from indicated mice at 2 weeks of age were stained with FITC-conjugated anti-CD4, anti-CD8, or PNA (green) and biotin-labeled anti-B220 followed by Texas red-conjugated avidin (red). Scale bars, 1 cm in C and 100 μm in others. *P < .05.

2.5-week-old mice. Although GC size was slightly increased in the spleen of 3-week-old NTx-PD-1$^{-/-}$ mice, localization of CD4$^+$ T cells moved into the marginal region of follicles (Figure 2A, right panels).

The rapid accumulation of CD4$^+$ T cells in the follicles with GC formation depended on concurrent loss of naturally arising Tregs and PD-1–mediated signaling because neither PD-1$^{-/-}$ mice nor NTx mice at 2 weeks of age showed any of these phenotypes (Figure 1F) nor did they develop fatal AIH.[3] In addition, Foxp3 expression of splenic CD4$^+$ T cells of NTx-PD-1$^{-/-}$ mice was severely reduced (Figure 2B), and transfer of Tregs from either normal BALB/c or PD-1$^{-/-}$ mice into NTx-PD-1$^{-/-}$ mice suppressed GC formations in the spleen (Figure 2C and data not shown). On the other hand, concomitant administration of blocking mAbs to programmed cell dealth 1 ligand (PD-L)1 and PD-L2 induced an accumulation of CD4$^+$ T cells in the follicles and development of GCs in the spleen of NTx mice at 2 weeks (Figure 2D). Interestingly, we found that, in one of the PD-1 ligands, PD-L1 messenger RNA (mRNA) expression was up-regulated in the liver of 1- to 3-week-old NTx-PD-1$^{-/-}$ mice (Figure 2E).

Splenic CD4$^+$ T Cells in NTx-PD-1$^{-/-}$ Mice Display the Molecular Signature of T_{FH} Cells and Directly Induce AIH

We next examined whether accumulated CD4$^+$ T cells in the follicles of the spleen display the molecular signature of T_{FH} cells. CD4$^+$ T cells in the spleen of 1-week-old NTx-PD-1$^{-/-}$ mice showed increased IL-21 mRNA expression (Figure 3A). In addition, CD4$^+$ T cells isolated from the spleen of 2- to 3-week-old NTx-PD-1$^{-/-}$ mice also showed increased Bcl-6 and IL-21 mRNA expressions (Figure 3B). Protein expressions of Bcl-6, IL-21, ICOS, and CXCR5 were detectable in these cells (Figure 3C and D, upper panels), indicating some key features of T_{FH} cells.[7-9] In addition, B220$^+$ B cells expressed FAS and GL7 (Figure 3D, lower panels), hallmarks of GC B cells.[7-9] Moreover, GC size increased in the spleen of mice aged 1 to 3 weeks (Supplementary Figure 2). Three-week-old NTx-PD-1$^{-/-}$ mice showed hyper-γ-globulinemia and vast production of class-switched ANAs (Supplementary Figure 3).

To investigate whether splenic T_{FH} cells directly trigger the development of T cell–mediated AIH, we purified ICOS$^+$CD4$^+$ T_{FH} cells or ICOS$^-$CD4$^+$ T cells from the spleen of 2.5-week-old NTx-PD-1$^{-/-}$ mice and transferred those T cells into T- and B cell–deficient RAG2$^{-/-}$ mice. In contrast to transfer of ICOS$^-$CD4$^+$ T cells, transfer of ICOS$^+$CD4$^+$ T_{FH} cells induced mononuclear cell infiltrations in the portal area of the liver and significantly increased serum levels of aspartate aminotransferase and alanine aminotransferase in recipient mice at 3 weeks after transfer (Figure 3E and F). These data suggest that splenic T_{FH} cells in NTx-PD-1$^{-/-}$ mice can directly trigger T cell–mediated AIH.

Key Features of T_{FH} Cells, Expressions of IL-21 and Bcl6 Are Sustained in Splenic and Hepatic CD4$^+$ T Cells in the Development of AIH

To further characterize CD4$^+$ T cell subsets in the development of AIH, we isolated splenic and hepatic CD4$^+$ T cells from NTx-PD-1$^{-/-}$ mice aged 1 to 3 weeks and measured expression levels of mRNA encoding master regulators and related cytokines for different T-cell subsets. Although not only T_{FH} cells but also T helper (Th) 17 cells are reported to express IL-21,[12] isolated CD4$^+$ T cells from the spleen and liver showed up-regulated IL-21 but not IL-17A mRNA expression in NTx-PD-1$^{-/-}$ mice (Figure 4A), suggesting that these CD4$^+$ T cells are not likely to be a Th17 subset. When we looked at master regulators for T-cell subsets, in NTx-PD-1$^{-/-}$ mice at 1 week, splenic CD4$^+$ T cells significantly up-regulated mRNA expression of Bcl-6 but not RORγT, GATA-3, or T-bet (Figure 4B). In addition, in the induction phase of AIH in NTx-PD-1$^{-/-}$ mice at 2 weeks, not only splenic CD4$^+$ T cells but also hepatic CD4$^+$ T cells significantly up-regulated mRNA expression of Bcl-6 but not others. Notably, although T-bet expression was also significantly up-regulated in both splenic and hepatic CD4$^+$ T cells in the progression phase of AIH in NTx-PD-1$^{-/-}$ mice at 3 weeks, up-regulated expression of Bcl-6 was sustained in those CD4$^+$ T cells.

Administration of Either Anti-ICOS or Anti–IL-21 Completely Suppresses Not Only T_{FH}-cell Generation but Also Induction of Fatal AIH

IL-12 is decisive in the development of Th1 subsets, whereas ICOS and IL-21 are indispensable for T_{FH}-cell differentiation and maturation.[7-9] To examine further whether differentiation of Th1 and/or T_{FH} subsets is critical in the induction of AIH, we administered blocking mAbs to IL-12p40, ICOS, or IL-21. Although production of ANA in both immunoglobulin (Ig)G1 and IgG2a subclasses increased in NTx-PD-1$^{-/-}$ mice (Supplementary Figure 3), injections of anti–IL-12p40 induced reciprocal alteration of ANA in Th1-dependent IgG2a and Th2-dependent IgG1 subclasses (Supplementary Figure 4). However, the neutralization of IL-12 did not significantly reduce the size of GCs in the spleen at 4 weeks (Figure 4C). In contrast, after 4 injections of either anti-ICOS or anti–IL-21, NTx-PD-1$^{-/-}$ mice at 4 weeks showed markedly suppressed GC formation in the spleen and accumulation of CD4$^+$ T cells in the follicles (Figures 4C and D and Supplementary Figures 5A and 6A). In addition, hyper-γ-globulinemia and ANA production, including class-switched Abs, were greatly reduced in those mice (Supplementary Figure 5C, and data not shown). Importantly, although neutralizing IL-12 did not suppress AIH development, either anti-ICOS or anti–IL-21 injections completely suppressed infiltration of not only
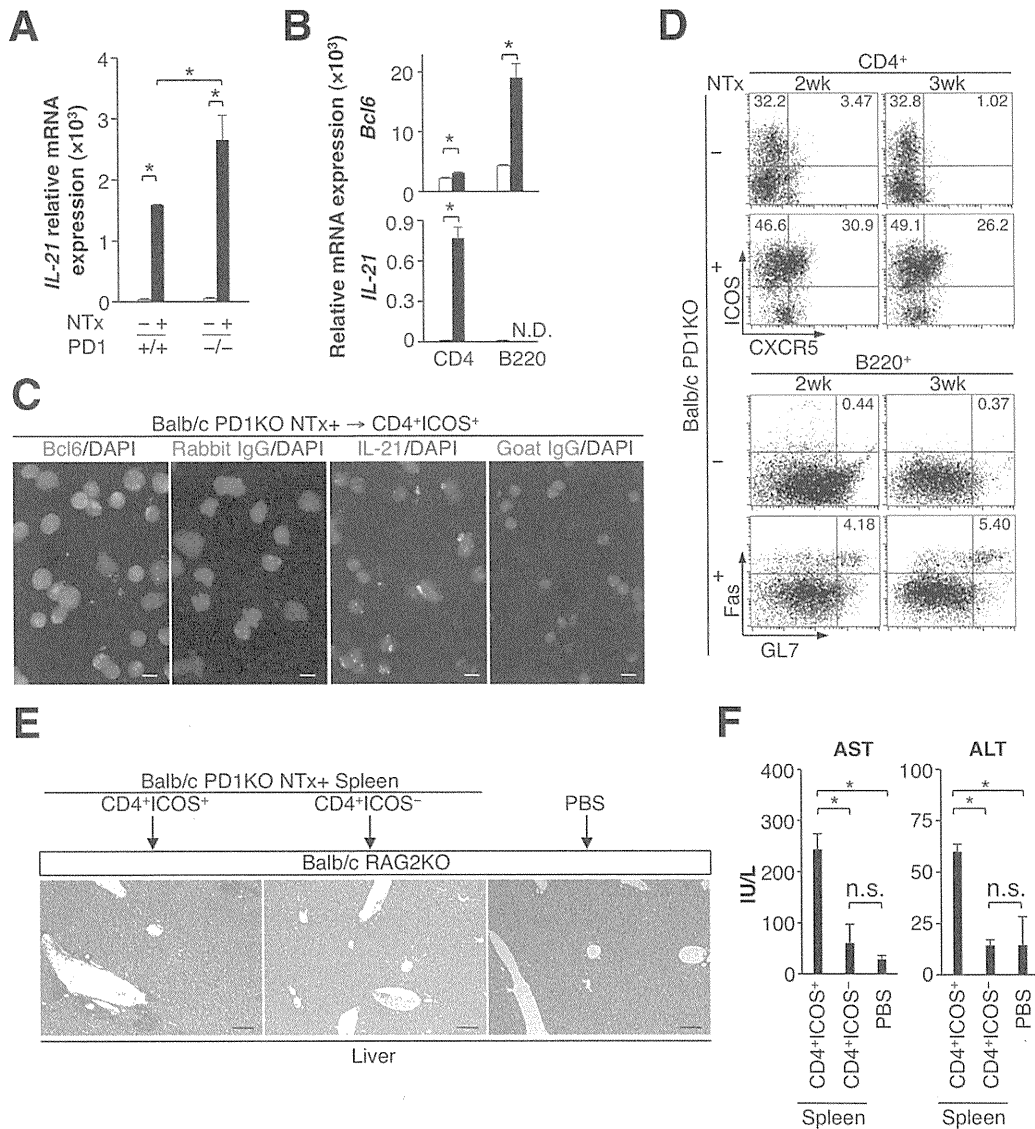
Figure 3. Splenic CD4$^+$ T cells in NTx-PD-1$^{-/-}$ mice display the molecular signature of T$_{FH}$ cells and directly trigger AIH. (*A*) IL-21 mRNA expressions by isolated splenic CD4$^+$ T cells in indicated mice at 1 week of age. (*B*) Bcl6 and IL-21 mRNA expressions by isolated splenic CD4$^+$ T cells and B220$^+$ B cells in 2.5-week-old PD-1$^{-/-}$ mice with (*solid columns*) or without (*open columns*) NTx. (*C*) Double immunostainings of isolated splenic CD4$^+$ICOS$^+$ T cells from 2.5-week-old NTx-PD-1$^{-/-}$ mice with DAPI and anti-Bcl6, anti–IL-21, or the isotype controls. (*D*) Flow cytometric analysis of CD4$^+$ T cells (*upper panels*) and B220$^+$ cells (*lower panels*) in indicated mice at 2 or 3 weeks of age. The cells were stained with indicated Abs as described in the Materials and Methods section. Numbers in *plots* indicate percent cells in each gate. (*E and F*) CD4$^+$ICOS$^+$ T cells or CD4$^+$ICOS$^-$ T cells from the spleen of 2.5-week-old NTx-PD-1$^{-/-}$ mice were transferred into RAG2$^{-/-}$ mice intravenously. (*E*) Staining of the liver for H&E 3 weeks after transfer. (*F*) Serum levels of the liver transaminase, aspartate aminotransferase (AST), and alanine aminotransferase (ALT). *Bars* indicate the mean of each group, and *horizontal short bars* indicate the standard deviation. *P < .05. N.D., not detected; n.s., not significant. *Scale bars*, 10 μm in C and 100 μm in others.

CD4$^+$ T cells but also CD8$^+$ T cells in the liver as well as liver destruction, resulting in a significantly higher survival rate (Figure 4*D-F* and Supplementary Figures 5*B* and 6*B*). These data suggest a link between generation of T$_{FH}$ cells and induction of AIH.

IL-21 Is a Key Cytokine for Not Only T$_{FH}$ Generation but Also Activation of CD8$^+$ T Cells

Next, we examined how CD4$^+$ T cells help CD8$^+$ T cells in developing AIH. In the induction phase in 2-week-old mice, CD8$^+$ T cells not only in the liver but

also in the spleen showed Ki-67^{high} activated T-cell phenotype with highly proliferating potential (Figure 5*A*). IL-21 potentially modulates activity of CD8$^+$ T cells,[11] and T$_{FH}$ cells in the spleen produced IL-21 (Figures 3*A-C* and 4*A*). Moreover, IL-21R mRNA expression in splenic CD8$^+$ T cells was elevated in NTx-PD-1$^{-/-}$ mice (Figure 5*B*). Therefore, to examine whether CD4$^+$ T-cell help for CD8$^+$ T-cell activation in the spleen depends on IL-21 in the induction phase of AIH, CD8$^+$ T cells were purified from the spleen of PD-1$^{-/-}$ mice. These CD8$^+$ T cells were cultured with CD4$^+$ T cells from the spleen of
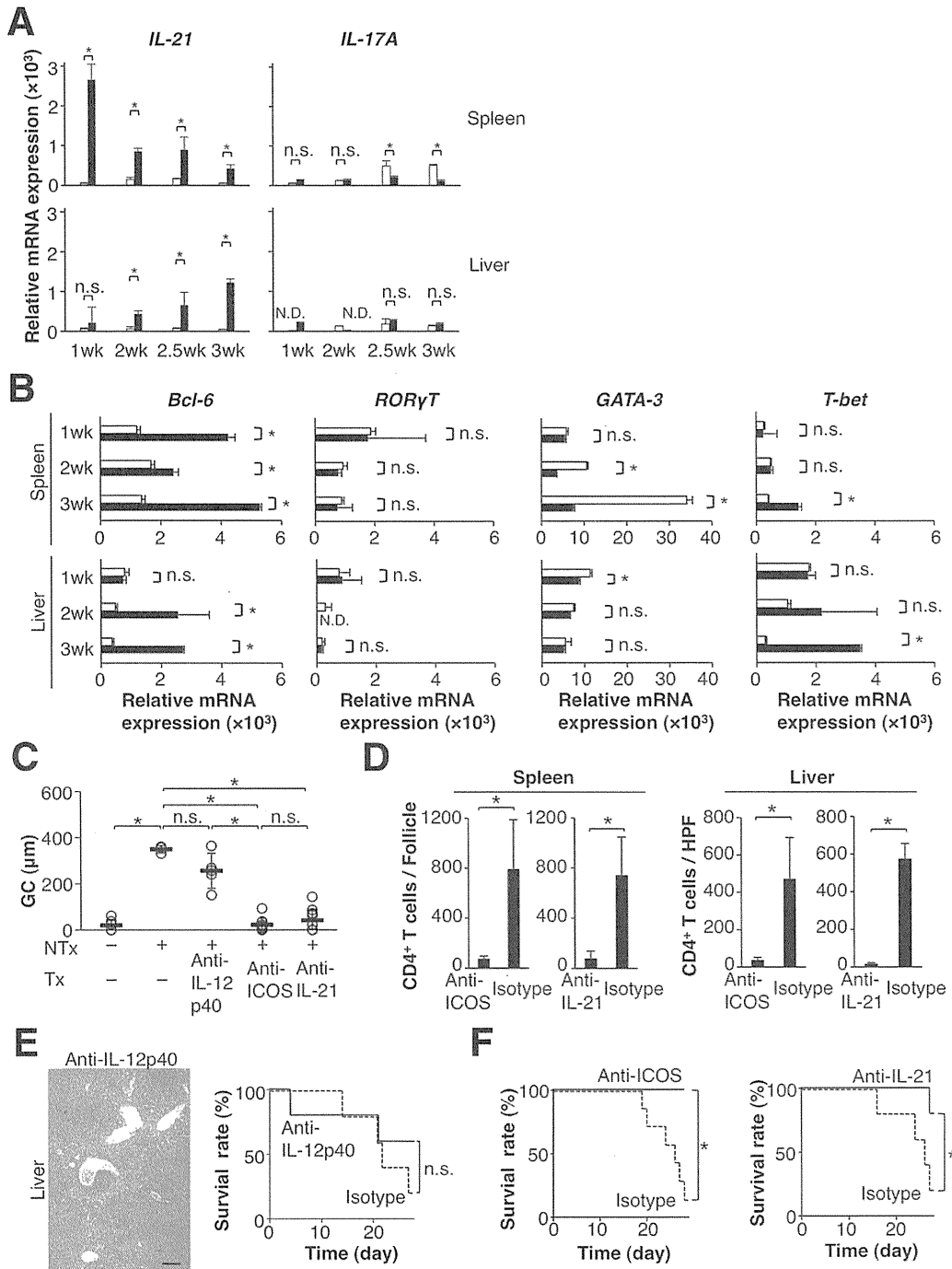
Figure 4. T_FH-cell generation rather than Th1 differentiation is primarily involved in the induction of fatal AIH. (*A* and *B*) Splenic and hepatic CD4$^+$ T cells were isolated from indicated aged PD-1$^{-/-}$ mice with (*solid columns*) or without (*open columns*) NTx. Real-time quantitative RT-PCR analysis was performed to measure the expression levels of mRNA encoding indicated master regulators for T-cell subsets and related cytokines. (*C–F*) NTx-PD-1$^{-/-}$ mice were intraperitoneally injected as described in Figure 1*B* with anti–IL-12p40, anti-ICOS, or anti–IL-21 Abs. After 4 injections, mice at 4 weeks of age were killed, and the spleens and livers were harvested. In *panel C*, the size of GCs in the spleen of indicated mice is shown. Spleens were stained as in Figure 1*F*. (*C*) Each *open circle* represents a size of GC measured in high-power fields. (*D*) CD4$^+$ T-cell numbers in the follicles of the spleen (*left*) or the liver (*right*) of indicated mice. (*E*) H&E staining of the liver and survival rate in NTx-PD-1$^{-/-}$ mice injected with anti–IL-12p40 (n = 5) or isotype (n = 5) Abs. (*F*) Survival rate in NTx-PD-1$^{-/-}$ mice with anti-ICOS (n = 5) or isotype (n = 7) Abs and those with anti–IL-21 (n = 5) or isotype (n = 5) Abs. *Bars* indicate the mean of each group, and *short bars* indicate the standard deviation. *$P < .05$. N.D., not detected; n.s., not significant. All *scale bars*, 100 μm.
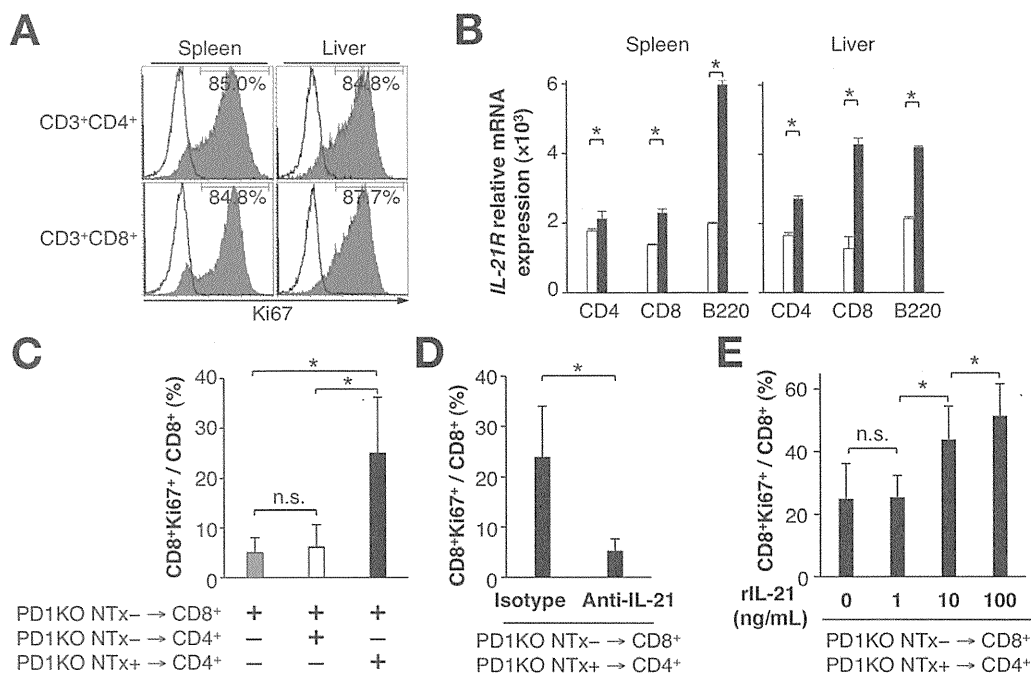
Figure 5. IL-21 is a key cytokine for CD8^{+} T-cell activation induced by CD4^{+} T cells. (A) Flow cytometric analysis of cells in the spleen and liver of 2-week-old NTx-PD-1^{−/−} mice. Phenotypes of CD3^{+}CD4^{+} and CD3^{+}CD8^{+} T cells were shown. Solid histograms represent anti–Ki-67 staining; open histograms represent the isotype controls. Numbers indicate percent of Ki67^{+} cells. Data represent 1 of 3 separate experiments. (B) IL-21R mRNA expressions by isolated CD4^{+}, CD8^{+} T cells, and B220^{+} B cells of the spleen and liver in 2.5-week-old PD-1^{−/−} mice with (solid columns) or without (open columns) NTx. Bars indicate the mean of each group, and horizontal short bars indicate the standard deviation. (C–E) Flow cytometric analysis of CD8^{+} T cells. CD8^{+} T cells were purified from the spleen of PD-1^{−/−} mice and then cultured with CD4^{+} T cells from the spleen of 2-week-old PD-1^{−/−} mice with or without NTx. After 1 day of culture with indicated conditions, percent of Ki67^{+} cells in CD8^{+} T-cell population was determined by flow cytometry. Bars indicate the mean of triplicated wells of each group, and horizontal short bars indicate the standard deviation. *P < .05. n.s., not significant.

2-week-old PD-1^{−/−} mice with or without NTx. After 1 day of culture, CD8^{+} T cells cultured with CD4^{+} T cells from NTx-PD-1^{−/−} mice showed a significant increase of Ki67^{+} cells in the CD8^{+} T-cell population, indicating that activated CD4^{+} T cells in the spleen of NTx-PD-1^{−/−} mice have the potential to induce CD8^{+} T-cell activation (Figure 5C). In addition, neutralizing antibodies to IL-21 suppressed increase of Ki67^{+} cells in CD8^{+} T-cell population cultured with those CD4^{+} T cells, suggesting that IL-21 produced by T$_{FH}$ cells drives activation of CD8^{+} T cells (Figure 5D). Moreover, recombinant IL-21 further increased Ki67^{+}CD8^{+} T cells cultured with those CD4^{+} T cells dose dependently (Figure 5E). These data suggest that IL-21 is a key cytokine for not only T$_{FH}$ generation but also activation of CD8^{+} T cells in AIH development.

The CCR6-CCL20 Axis Is Crucial for Splenic T-Cell Migration Into the Liver, Inducing Fatal AIH

Finally, to examine how dysregulated T$_{FH}$ cells and activated CD8^{+} T cells migrate from the spleen into the liver in the induction phase of AIH, we analyzed chemokine receptor expression of T cells in the spleen and liver by flow cytometry. Previously, we showed that CD4^{+} T cells in the spleen and liver expressed chemokine receptor CCR6 in NTx-PD-1^{−/−} mice.[3] In CD4^{+} T cells of 2-week-old NTx-PD-1^{−/−} mice, CCR6^{+} and, to a lesser extent, CCR9^{+} cells increased (Figure 6A). The predominant increase of CCR6^{+} cells was observed only at 2 weeks in the spleen and liver but not in mesenteric lymph nodes. In contrast, in 3-week-old mice, CXCR3^{+} cells were predominant in splenic and hepatic CD4^{+} T cells compared with CCR6^{+} or CCR9^{+} cells (Figure 6B). Splenic CCR6^{+}CD4^{+} T cells in NTx-PD-1^{−/−} mice contained CXCR5^{+}CCR6^{+} population (Figure 6C, left panels), suggesting that these T cells retained the molecular signature of T$_{FH}$ cells. In 3-week-old mice, CXCR5^{+}CCR6^{−} population was further increased, whereas the CXCR5[+or−]CCR6^{+} population was decreased (Figure 6C, right panels), suggesting preferential loss of CCR6^{+} cells from the spleen after induction of AIH. In addition to CD4^{+} T cells, in CD8^{+} T cells, predominant increases of CCR6^{+} cells in the spleen and liver were also found in the induction phase of AIH (Figure 6D and E). Moreover, gene expression of CCR6 ligand CCL20, but not CCR9 ligand CCL25, was elevated in the liver of 1.5- and 2-week-old NTx-PD-1^{−/−} mice (Figure 6F). These data suggest that CCR6-expressing T cells in the spleen may migrate into CCL20-expressing liver and trigger the development of fatal AIH.
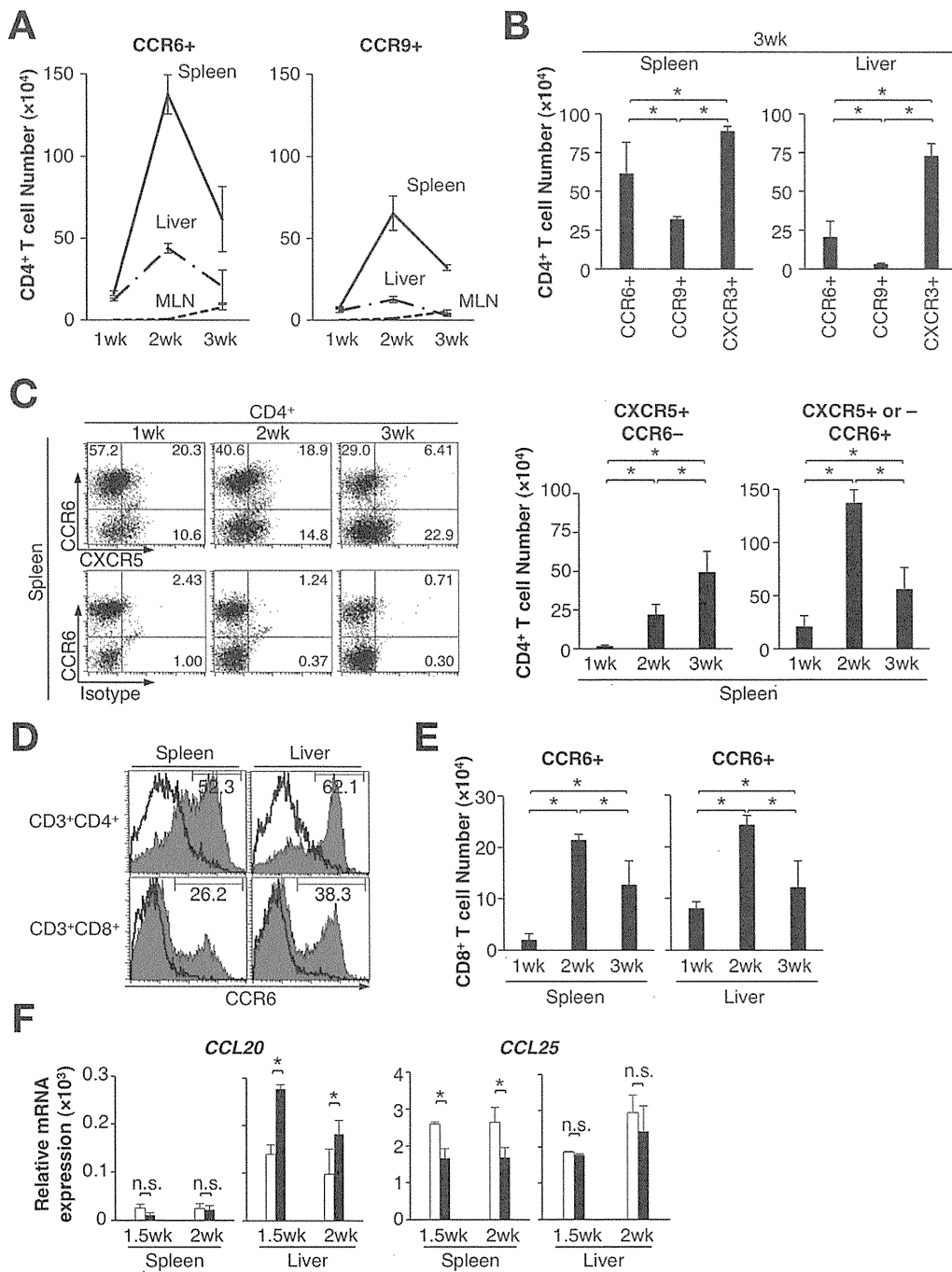
BASIC–LIVER, PANCREAS, AND BILIARY TRACT

Figure 6. CCR6$^+$ cells are predominantly increased in CD4$^+$ and CD8$^+$ T cells in the spleen and liver only in the induction phase of AIH. (*A–E*) Cells in the spleen, liver, and mesenteric lymph nodes (*MLN*) of NTx-PD-1$^{-/-}$ mice at the indicated age were stained with FITC-anti-CD3e, APC-Cy7-anti-CD4 and PE-anti-CCR6, -anti-CCR9, or -anti-CXCR3 (*A*, *B*, and *D*, *upper panels*), with FITC-anti-CXCR5, PE-anti-CCR6, and APC-Cy7-anti-CD4 (*C*), or with FITC-anti-CD3e, PE-anti-CCR6 APC-anti-CD8 (*D*, *lower panels*, and *E*). Flow cytometric analyses were assessed as in Figure 3D. Numbers of indicated T-cell populations were calculated by (percentage of the cells in viable cells) × (number of viable cells) (*A*, *B*, *C*, *right panels*, and *E*). *Numbers* indicate percent of indicated gates (*C*, *left panels*; *D*). (*F*) CCL20 or CCL25 mRNA expressions in the spleen and liver of PD-1$^{-/-}$ mice at indicated age with (*solid columns*) or without (*open columns*) NTx. *Bars* indicate the mean of each group, and *horizontal short bars* indicate the standard deviation. *$P < .05$. n.s., not significant.

To determine whether the CCR6-CCL20 axis is critical for migration of splenic T cells into the liver and triggering fatal AIH, we administered mAbs blocking to CCL20. After 3 injections of anti-CCL20 Abs, the spleen of 3-week-old NTx-PD-1$^{-/-}$ mice showed further accumulation of T$_{FH}$ cells in the GC$^+$ follicles diffusely (Figure 7A and B, *left panel*). These findings contrasted with the spleens of non-injected 3-week-old NTx-PD-1$^{-/-}$ mice, in which splenic
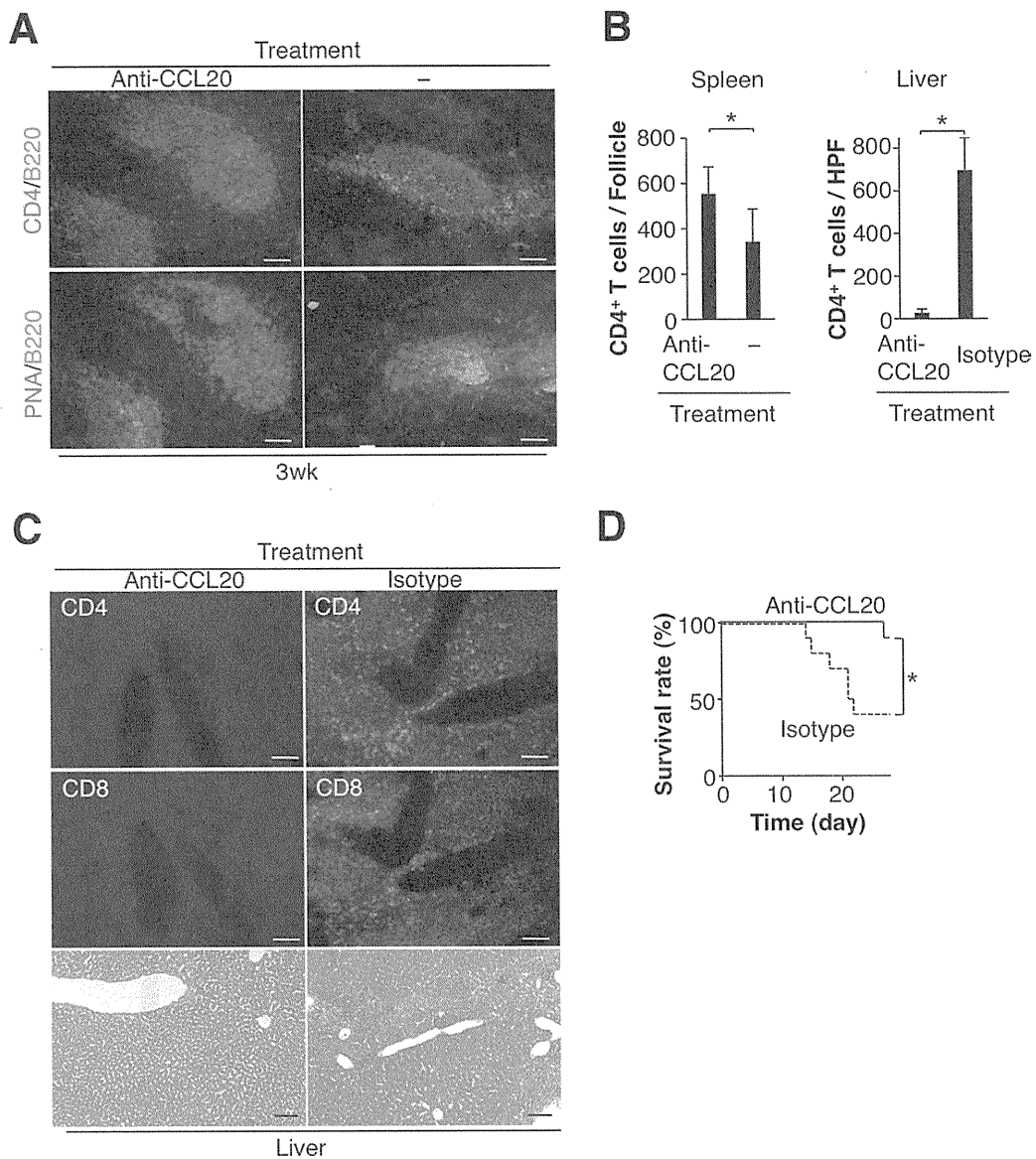
Figure 7. The CCR6-CCL20 axis plays a crucial role for both migration of splenic T_{FH} cells into the liver and induction of fatal AIH. (*A–D*) NTx-PD-1$^{-/-}$ mice were injected intraperitoneally as described in Figure 1 with anti-CCL20 (n = 10) or isotype (n = 10) Abs. The spleen and liver were stained as in Figure 1*B* and 1*F*. (*A*) Double immunostainings of the spleen of 3-week-old mice. (*B*) CD4$^+$ T-cell numbers in the follicles of the spleen of 3-week-old (*left*) and in the liver of 4-week-old (*right*) of indicated mice. (*C*) Immunostainings for CD4 and CD8 and H&E staining (*lower panels*) of the liver of 4-week-old mice. (*D*) Survival rate of each group of 4-week-old mice. *Bars* indicate the mean of each group, and *horizontal short bars* indicate the standard deviation. *P < .05. All *scale bars*, 100 μm.

T_{FH} cells were mainly localized in the marginal region of follicles (Figure 7*A*), and with the spleens from anti-ICOS or anti–IL-21 injected mice, in which splenic CD4$^+$ T cells were greatly reduced (Figure 4*D*). Importantly, administering anti-CCL20 suppressed infiltration of CD4$^+$ and CD8$^+$ T cells into the liver and liver destruction, with a significantly increased survival rate at 4 weeks (Figure 7*B*, *right panel*, 7*C* and *D*). These data suggest that, in the induction phase of AIH, the CCR6-CCL20 axis is crucial for migration of dysregulated T_{FH} cells and activated CD8$^+$ T cells from the spleen into the liver.

Discussion

We demonstrated herein that in our mouse model of spontaneous AIH induced by a concurrent loss of Tregs and PD-1–mediated signaling, splenic CD4$^+$ T cells are crucial in the development of fatal AIH. In the induction phase, splenic CD4$^+$ T cells in these mice showed the T_{FH}-cell phenotype, and CCR6-expressing T_{FH} cells and activated CD8$^+$ T cells in the spleen preferentially recruited to the liver via CCL20, triggering the induction of fatal AIH.

We found that $CD4^+$ T cells in the induction site of AIH, the spleen, were exclusively localized in GC-bearing B-cell follicles. In the induction phase of AIH, these $CD4^+$ T cells up-regulated expression of Bcl6, the master transcription factor for T_{FH}-cell differentiation, and showed the $IL-21^+IL-21R^+ICOS^+CXCR5^+$ T_{FH}-cell phenotype.[7-9] In addition, B cells in the spleen contained FAS^+GL7^+ GC B cells, and hyper-γ-globulinemia, and huge production of class-switched ANAs were observed in the serum from NTx-PD-$1^{-/-}$ mice. Moreover, in vivo administration of blocking Abs to ICOS or IL-21, indispensable for T_{FH}-cell generation and maturation,[7-9] inhibited accumulation of $CD4^+$ T cells in B-cell follicles and GC formation in the spleen, and suppressed hyper-γ-globulinemia, class-switched ANA production as well as induction of AIH. Importantly, adaptive transfer of the splenic T_{FH} cells from NTx-PD-$1^{-/-}$ mice directly triggered T cell–mediated AIH. From these data, we concluded that, in our mouse model, the responsible $CD4^+$ T-cell subset in the induction site of AIH is T_{FH} cells.

Previously, we reported that severely inflamed livers in 3-week-old NTx-PD-$1^{-/-}$ mice contained a massive infiltration of activated $CD4^+$ and $CD8^+$ T cells producing inflammatory cytokines, such as IFN-γ and tumor necrosis factor-α.[3] In contrast, we found in this study that in the induction phase of AIH, IL-21-producing splenic T_{FH} cells were responsible for the initiation of liver inflammation. Thus, dysregulated T_{FH} cells and Th1-like cells appear to operate at different time points in the development of fatal AIH. Recent studies show that, although in experimental autoimmune encephalomyelitis (EAE), a $CD4^+$ T cell–mediated disease of the central nervous system, Th1 cells are present in EAE lesions during its active phase, and, in its induction phase, Th17 cells directly initiate inflammation and trigger the entry of a second wave of Th1 cells that migrate into the EAE lesions.[13] Because we found up-regulation of bcl-6 and t-bet in both splenic and hepatic $CD4^+$ T cells of 3-week-old NTx-PD-$1^{-/-}$ mice, it might be that, in the progression phase of AIH, dysregulated T_{FH} cells directly differentiate into Th1-like cells in the spleen and give rise to the migration of a second wave of Th1-like cells into the liver.

In this mouse model, infiltration of both $CD4^+$ and $CD8^+$ T cells in the liver are required for progression to fatal AIH, and the infiltration of $CD8^+$ T cells in the liver depends on $CD4^+$ T cells. In the induction phase of AIH, splenic $CD8^+$ T cells showed Ki-67^{high} activated T-cell phenotype. $CD4^+$ T cells from the spleen of 2-week-old NTx-PD-$1^{-/-}$ mice induced IL-21-driven $CD8^+$ T-cell activation. In addition, activated $CD8^+$ T cells in the spleen expressed CCR6 and were preferentially recruited to the liver via CCL20. However, the precise roles of $CD8^+$ T cells in the induction phase of AIH are still unclear. Because a large number of $CD8^+$ T cells infiltrated into the liver during AIH progression, $CD8^+$ T cells infiltrated

in the induction phase might be involved in triggering the subsequent expansion and/or infiltration of inflammatory T cells in the progression phase.

We showed here that the CCR6-CCL20 axis is essential for splenic T_{FH} cells to migrate into the liver, triggering inflammation. CCR6 is also expressed on Th17 cells and is vital to the initiation of Th17-cell migration to target tissues.[13-15] CCR6 is expressed on not only Th17 cells but also Tregs in mice[14,15] and human T cells that produce both IL-17 and IFN-γ as well as Th1 cells.[16] Taken together, these data suggest that the CCR6-CCL20 axis plays an important role in the migration of instructed $CD4^+$ T cells into target tissues.

We also showed that NTx-PD-$1^{-/-}$ mice but not NTx mice at 2 weeks generated T_{FH} cells in the spleen. In addition, concomitant administration of blocking mAbs to PD-L1 and PD-L2 generated T_{FH} cells in the spleen of NTx mice at 2 weeks. Moreover, purified $CD4^+$ T cells in the spleen of 1-week-old NTx-PD-$1^{-/-}$ mice had greater IL-21 mRNA expression than those in NTx mice. In this regard, recent studies suggested that PD-1 deficiency increased T_{FH}-cell numbers but reduced IL-21 production by T_{FH} cells in long-term humoral immunity[17] and that T_{FH}-cell differentiation requires strong signals through the T-cell receptor.[18] Thus, in our model, PD-1 deficiency may induce enhanced production of IL-21 by activated autoreactive $CD4^+$ T cells to differentiate into T_{FH} cells in the induction phase. On the other hand, we found that PD-L1 but not PD-L2 mRNA expression was up-regulated in the liver of NTx-PD-$1^{-/-}$ mice. Because PD-1 and PD-1 ligands expressions are increased in the livers of most AIH patients,[19,20] it is possible that PD-1/PD-L1 interaction is insufficient to completely suppress liver inflammation but may halt progression to fatal AIH.

In humans, it is unknown at present whether the spleen is the induction site of AIH or T_{FH} cells are the T-cell subset responsible for induction of AIH. In patients with active AIH, splenomegaly is a common clinical finding. However, splenectomy for these patients has not been reported to be therapeutic. Therefore, splenectomy may help patients at the early phase of AIH but not those with more advanced cases. Notably, because patients with severe AIH have a high potential for recurrence after liver transplantation and the recurrence of AIH leads to a greater probability of graft loss,[21,22] splenectomy might be a therapeutic option to prevent recurrence after liver transplantation. On the other hand, it may be that dysregulated T_{FH} cells are involved in both B cell- and T cell–mediated autoimmunity in human AIH. Indeed, T_{FH} cells not only offer powerful help to B cells in forming germinal centers in humoral immunity but also induce B cell–mediated systemic autoimmunity in humans and mice.[7-9,23] In addition, although T_{FH} cells are mainly localized in B-cell follicles in lymphoid organs, circulating T cells resembling T_{FH} cells exist in the peripheral blood of patients with systemic lupus erythematosus.[10]

Furthermore, IL-21 secreted by effecter T cells including T_{FH} cells can modulate the activity of $CD8^+$ T cells and other immune and nonimmune cells in humans and mice.[11]

In conclusion, we demonstrated in the present study that Tregs and PD-1-mediated signaling are important in regulating T_{FH} cells and that dysregulated T_{FH} cells in the spleen are responsible for induction of fatal AIH in NTx-PD-1$^{-/-}$ mice. In addition, CCR6-CCL20 axis-dependent migration of T_{FH} cells is crucial for initiation of AIH. These data may lead to novel therapeutic approaches to human AIH, especially acute-onset fulminant AIH.

Supplementary Material

Note: To access the supplementary material accompanying this article, visit the online version of *Gastroenterology* at www.gastrojournal.org, and at doi: 10.1053/j.gastro.2011.01.002.

References

1. Krawitt EL. Autoimmune hepatitis. N Engl J Med 2006;354: 54–66.
2. Manns MP, Vogel A. Autoimmune hepatitis, from mechanisms to therapy. Hepatology 2006;43:S132–S144.
3. Kido M, Watanabe N, Okazaki T, et al. Fatal autoimmune hepatitis induced by concurrent loss of naturally arising regulatory T cells and PD-1-mediated signaling. Gastroenterology 2008;135:1333–1343.
4. Diamantis I, Boumpas DT. Autoimmune hepatitis: evolving concepts. Autoimmun Rev 2004;3:207–214.
5. Ichiki Y, Aoki CA, Bowlus CL, et al. T cell immunity in autoimmune hepatitis. Autoimmun Rev 2005;4:315–321.
6. Suzuki Y, Kobayashi M, Hosaka T, et al. Peripheral CD8+/CD25+ lymphocytes may be implicated in hepatocellular injuries in patients with acute-onset autoimmune hepatitis. J Gastroenterol 2004;39:649–653.
7. McHeyzer-Williams LJ, Pelletier N, Mark L, et al. Follicular helper T cells as cognate regulators of B cell immunity. Curr Opin Immunol 2009;21:266–273.
8. King C. New insights into the differentiation and function of T follicular helper cells. Nat Rev Immunol 2009;9:757–766.
9. Yu D, Batten M, Mackay CR, et al. Lineage specification and heterogeneity of T follicular helper cells. Curr Opin Immunol 2009;21:619–625.
10. Simpson N, Gatenby PA, Wilson A, et al. Expansion of circulating T cells resembling follicular helper T cells is a fixed phenotype that identifies a subset of severe systematic lupus erythematosus. Arthritis Rheum 2010;62:234–244.
11. Monteleone G, Pallone F, Macdonald TT. Interleukin-21 (IL-21)-mediated pathways in T cell-mediated disease. Cytokine Growth Factor Rev 2009;20:185–191.
12. Korn T, Bettelli E, Oukka M, et al. IL-17 and Th17 cells. Annu Rev Immunol 2009;27:485–517.
13. Reboldi A, Coisne C, Baumjohann D, et al. C-C chemokine receptor 6-regulated entry of TH-17 cells into the CNS through the choroid plexus is required for the initiation of EAE. Nat Immunol 2009;10:514–523.
14. Hirota K, Yoshitomi H, Hashimoto M, et al. Preferential recruitment of CCR6-expressing Th17 cells to inflamed joints via CCL20 in rheumatoid arthritis and its animal model. J Exp Med 2007; 204:2803–2812.
15. Yamazaki T, Yang XO, Chung Y, et al. CCR6 regulates the migration of inflammatory and regulatory T cells. J Immunol 2008;181: 8391–8401.
16. Acosta-Rodriguez EV, Rivino L, Geginat J, et al. Surface phenotype and antigenic specificity of human interleukin 17-producing T helper memory cells. Nat Immunol 2007;8:639–646.
17. Good-Jacobson KL, Szumilas CG, Chen L, et al. PD-1 regulates germinal center B cell survival and the formation and affinity of long-lived plasma cells. Nat Immunol 2010;11:535–542.
18. Fazilleau N, McHeyzer-Williams LJ, Rosen H, et al. The function of follicular helper T cells is regulated by the strength of T cell antigen receptor binding. Nat Immunol 2009;10:375–384.
19. Oikawa T, Takahashi H, Ishikawa T, et al. Intrahepatic expression of the co-stimulatory molecules programmed death-1, and its ligands in autoimmune liver disease. Pathol Int 2007;57:485–492.
20. Kassel R, Cruise MW, Iezzoni JC, et al. Chronically inflamed livers up-regulate expression of inhibitory B7 family members. Hepatology 2009;50:1625–1637.
21. Vogel A, Heinrich E, Bahr MJ, et al. Long-term outcome of liver transplantation for autoimmune hepatitis. Clin Transplant 2004; 18:62–69.
22. Rowe IA, Webb K, Gunson BK, et al. The impact of disease recurrence on graft survival following liver transplantation: a single centre experience. Transpl Int 2008;21:459–465.
23. Linterman MA, Rigby RJ, Wong RK, et al. Follicular helper T cells are required for systemic autoimmunity. J Exp Med 2009;206: 561–576.

BASIC–LIVER, PANCREAS, AND

Supplementary Materials and Methods

Mice

BALB/c mice were purchased from Japan SLC (Shizuoka, Japan), and programmed cell death 1 (PD-1)$^{-/-}$ and RAG2$^{-/-}$ mice on a BALB/c background were generated as described.[1,2] All of these mice were bred and housed under specific pathogen-free conditions. Thymectomy and splenectomy of the mice 3 days after birth were performed as described.[3,4] All mouse protocols were approved by the Institute of Laboratory Animals, Graduate School of Medicine, Kyoto University.

Enzyme-Linked Immunosorbent Assay

Serum immunoglobulin (Ig) levels were determined by enzyme-linked immunosorbent assay (ELISA) as described,[5] and antibody (Ab) sets for detection of mouse IgG1, IgG2a, IgG2b, IgG3, IgA, and IgE from BD Biosciences (San Jose, CA) and anti-mouse IgM from AbD Serotec (Oxford, UK) were used. To detect serum antinuclear antibody (ANA), microtiter plates (Nunc, Roskilde, Denmark) were incubated with 10 μg/mL antigens, and the nuclear fraction was prepared from normal liver.[6] Ab sets for detection of mouse ANA subclasses were the same as above.

Administration of Abs in Vivo

PD-1–deficient BALB/c mice thymectomized 3 days after birth (NTx-PD-1$^{-/-}$ mice) at 1 day after thymectomy were intraperitoneally injected every week with 100 μg of Abs. Anti-CD4 (RM4-5) and anti-CD8 (53-6.7) for depletion of CD4$^+$ T cells and CD8$^+$ T cells, respectively, and neutralizing Abs to mouse inducible costimulator (ICOS) (7E.17G9) were from eBioscience (San Diego, CA). Neutralizing Abs to mouse interleukin (IL)-21 (AF594) and IL-12p40 (C17.8) as well as CCL20 (114908) were from R&D Systems (Minneapolis, MN). Neutralizing Abs to mouse PD-L1 and PD-L2 were purified from ascites as described.[7] All isotypes were from eBioscience or R&D Systems (Minneapolis, MN). After 2 to 4 injections, mice at 2 to 4 weeks of age were killed, and their spleens and livers were harvested.

Histologic and Immunohistologic Analysis

Organs were fixed in neutral buffered formalin and embedded in paraffin wax. Sections were stained with H&E for histopathology. Fluorescence immunohistology was performed on frozen sections as described previously[3] using fluorescein isothiocyanate (FITC)-conjugated anti-CD4 (RM4-5), anti-CD8a (Ly-2) (eBioscience), peanut agglutinin (PNA; Vector Laboratories, Burlingame, CA), and biotin-labeled anti-B220 (RA3-6B2) (BD Biosciences) followed by Texas red-conjugated avidin (Vector Laboratories). Numbers of CD4$^+$ T cells localized within B220$^+$ B-cell follicles in the spleen and inflamed liver were counted in several high-power fields in at least

3 sections of each mouse. Diameter of germinal center (GC) was measured in several high-power fields in at least 3 sections of each mouse. Single-cell suspensions of isolated splenic CD4$^+$ICOS$^+$ T cells from 2.5-week-old NTx-PD-1$^{-/-}$ mice were mounted on glass slides by cytocentrifuge preparation. After fixation, these cells were stained with anti-Bcl6 (N3) (Santa Cruz Biotechnology, Santa Cruz, CA) followed by FITC-conjugated goat anti-rabbit Ig (BD Biosciences) or anti–IL-21 (AF594) (R&D Systems) followed by FITC-conjugated rabbit anti-goat Ig (ab6737) (Abcam, Cambridge, MA), and DAPI (Sigma-Aldrich, St. Louis, MO). Rabbit IgG isotype (DA1E) and normal goat IgG isotype (AB-108-C) were from Cell Signaling (Danvers, MA) and from R&D Systems, respectively.

Flow Cytometry Analysis and Isolation of Lymphocytes

Single cells from the livers and spleens were prepared as described.[3] The following mAbs were used for staining: FITC-conjugated anti-CD3e (145-2C11), anti-CD8a (eBioscience); anti-CXCR5 (2G8), anti-GL7, anti-Ki67 (B56) (BD Biosciences); PE-conjugated anti-CD3e, anti-CD4, anti-CD25 (PC61.5), anti-ICOS (eBioscience); anti-B220, anti-CD95/Fas (Jo2) (BD Biosciences); anti-CCR6 (140706), anti-CCR9 (242503), anti-CXCR3 (220803) (R&D Systems); APC-Cy7-conjugated anti-CD4 (GK1.5), biotin-labeled B220 (BD Biosciences); and allophycocyanin (APC)-conjugated streptavidin, and anti-CD8a (eBioscience). In flow cytometric analysis of CD4$^+$ T cells and B220$^+$ B cells in Figure 3, cells were stained with FITC-anti-CXCR5, PE-anti-ICOS, and APC-Cy7-anti-CD4 for CD4$^+$ T cells, or with FITC-anti-GL7, PE-anti-CD95/Fas, and biotin-labeled B220 followed by APC-conjugated streptavidin for B220$^+$ B cells. For Ki-67 antigen staining in Figure 5, a FITC-conjugated Ab set (BD Bioscience) was used with PE-anti-CD3 and APC-Cy7-anti-CD4 or APC-anti-CD8. In flow cytometric analysis of T cells in Figure 6, cells were stained with FITC-anti-CD3e, PE-anti-CCR6, -anti-CCR9, or -anti-CXCR3 and APC-Cy7-anti-CD4, with FITC-anti-CXCR5, PE-anti-CCR6, and APC-Cy7-anti-CD4, or with FITC-anti-CD3e, PE-anti-CCR6, and APC-anti-CD8. Stained cells were analyzed with a FACSCanto II (BD Biosciences). Data were analyzed using Cell Quest Pro (BD Biosciences). Dead cells were excluded on the basis of side- and forward-scatter characteristics, and viable T-cell numbers were calculated as follows: (the percentage of cells in the cell type) $\times$ (the number of viable cells). CD3$^+$CD4$^+$, CD3$^+$CD8$^+$, CD3$^-$B220$^+$ cells from the spleen or liver, and CD4$^+$ICOS$^+$, CD4$^+$ICOS$^-$ T cells and CD4$^+$CD25$^+$ T regulatory cells (Tregs) from the spleen were obtained by a FACS Aria II (BD Biosciences) to reach >99% purity, as described.[3]

Adoptive Transfer

CD4$^+$CD25$^+$ Tregs were prepared from the spleen of adult BALB/c PD-1$^{+/+}$ or PD-1$^{-/-}$ mice as described.[3] Tregs (1 × 10^6) were intraperitoneally injected into NTx-PD-1$^{-/-}$ mice at 1 day after thymectomy. For transfer of follicular helper T (T$_{FH}$) cells or non-T$_{FH}$ cells, CD4$^+$ICOS$^+$ T cells or CD4$^+$ICOS$^-$ T cells, respectively, were prepared from the spleen of 2.5-week-old NTx-PD-1$^{-/-}$ mice as described above. Isolated T cells (1 × 10^6) were intravenously injected into RAG2-deficient recipient mice on a BALB/c background at 4 weeks of age. Three weeks after transfer, recipient mice were examined.

Real-Time Quantitative Reverse-Transcription Polymerase Chain Reaction

Real-time quantitative reverse-transcription polymerase chain reaction was performed as described previously.[8] Spleen and liver tissues or isolated lymphocytes were frozen in RNA later. RNA was prepared with an RNeasy mini kit (Qiagen, Hilden, Germany), and single-strand complementary DNA (cDNA) was synthesized with SuperScript II reverse transcriptase (Invitrogen, Carlsbad, CA). Real-time quantitative reverse-transcription polymerase chain reaction was performed using SYBR Green I Master (Roche Applied Science, Basel, Switzerland). The real-time quantitative reactions were performed using a Light Cycler 480 (Roche Applied Science) according to the manufacturer's instructions. Values are expressed as arbitrary units relative to glyceraldehyde-3-phosphate dehydrogenase (GAPDH). The following primers were used: *GAPDH*: 5'-CAACTTTGTCA AGCTCATTTCC-3' and 5'-GGTCCAGGGTTTCTTA CTCC-3'; *PD-L1*: 5'-GGAATTGTCTCAGAATGGTC-3' and 5'-GTAGTTGCTTCTAGGAAGGAG-3'; *PD-L2*: 5'-GCATGTTCTGGAATGCTCAC-3' and 5'-CTTTGGGT TCCATCCGACT-3'; *Foxp3*: 5'-TCAGGAGCCCACC AGTACA-3' and 5'-TCTGAAGGCAGAGTCAGGAGA-3'; *Bcl6*: 5'-ACACATGCAGGAAGTTCATCAAGG-3' and 5'-CATATTGTTCTCCACGACCTCACG-3'; *IL-21*: 5'-GACATTCATCATCGACCTCGT-3' and 5'-TCACAGG AAGGGCATTTAGC-3'; *IL-21R*: 5'-AGTGACCCCGTCAT CTTTCA-3' and 5'-AGGAGCAGCAGCATGTGAG-3'; *RORγT*: 5'-CCGCTGAGAGGGCTTCAC-3' and 5'-TG CAGGAGTAGGCCACATTACA-3'; *IL-17A*: 5'-CTCCA GAAGGCCCTCAGACTAC-3' and 5'-AGCTTTCCCTC CGCATTGACACAG-5'; *T-bet*: 5'-TCAACCAGCACCAGA CAGAG-3' and 5'-AAACATCCTGTAATGGCTTGTG-3';

GATA-3: 5'-TTATCAAGCCCAAGCGAAG-3' and 5'-TG GTGGTGGTCTGACAGTTC-3'; *CCL20*: 5'-ATGGCCTG CGGTGGCAAGCGTCT-3' and 5'-TAGGCTGAGGAG GTTCACAGCCC-3'; *CCL25*: 5'-GAGTGCCACCCTAG GTCATC-3' and 5'-CCAGCTGGTGCTTACTCTGA-3'.

T-Cell Coculture

CD4$^+$ and CD8$^+$ T cells were isolated from the spleen of 2-week-old PD-1$^{-/-}$ mice with or without neonatal thymectomy (NTx) using a FACS Aria II (BD Biosciences) to reach >99% purity, as described.[3] Isolated CD8$^+$ T cells (5 × 10^5) were cocultured with 5 × 10^5 freshly isolated CD4$^+$ T cells in round-bottomed, 96-well culture plates in Dulbecco's modified Eagle medium supplemented with 10% fetal bovine serum, 50 mmol/L 2-mercaptoethanol, 100 U/mL penicillin, and 100 μg/mL streptomycin. In some experiments, we used the following reagents in these culture conditions: 10 μg/mL of anti–IL-21 (AF594), 10 μg/mL of goat IgG isotype, and 1–100 ng/mL of recombinant IL-21 (all from R&D Systems). After 24 hours of culture, cells were stained with PE-anti-CD3, APC-anti-CD8, and FITC-anti-Ki67 or -isotype control and analyzed with a FACSCanto II.

References

1. Nishimura H, Okazaki T, Tanaka Y, et al. Autoimmune dilated cardiomyopathy in PD-1 receptor-deficient mice. Science 2001; 291:319–322.
2. Shinkai Y, Rathbun G, Lam KP, et al. RAG-2-deficient mice lack mature lymphocytes owing to inability to initiate V(D)J rearrangement. Cell 1992;68:855–867.
3. Kido M, Watanabe N, Okazaki T, et al. Fatal autoimmune hepatitis induced by concurrent loss of naturally arising regulatory T cells and PD-1-mediated signaling. Gastroenterology 2008;135:1333–1343.
4. Klonowski KD, Marzo AL, Williams KJ, et al. CD8 T cell recall responses are regulated by the tissue tropism of the memory cell and pathogen. J Immunol 2006;177:6738–6746.
5. Muramatsu M, Kinoshita K, Fagarasan S, et al. Class switch recombination and hypermutation require activation-induced cytidine deaminase (AID), a potential RNA editing enzyme. Cell 2000; 102:553–563.
6. Blobel G, Potter VR. Nuclei from rat liver: isolation method that combines purity with high yield. Science 1966;154:1662–1665.
7. Ishida M, Iwai Y, Tanaka Y, et al. Differential expression of PD-L1 and PD-L2, ligands for an inhibitory receptor PD-1, in the cells of lymphohematopoietic tissues. Immunol Lett 2002;84:57–62.
8. Kido M, Tanaka J, Aoki N, et al. *Helicobacter pylori* promotes the production of thymic stromal lymphopoietin by gastric epithelial cells and induces dendritic cell-mediated inflammatory Th2 responses. Infect Immun 2010;78:108–114.
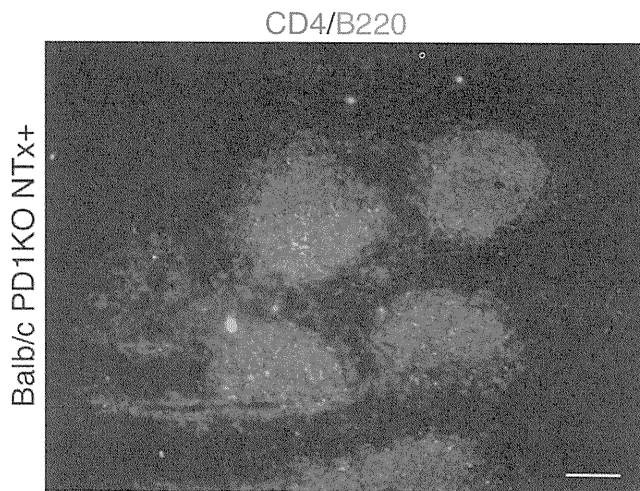
Supplementary Figure 1. Splenic CD4$^+$ T cells are preferentially localized within B220$^+$ B-cell follicles in the induction phase of AIH in NTx-PD-1$^{-/-}$ mice. The spleens from 2-week-old NTx-PD-1$^{-/-}$ mice were stained with biotin-labeled anti-B220 and FITC-conjugated anti-CD4 followed by Texas red-conjugated avidin. *Scale bar*, 100 μm.
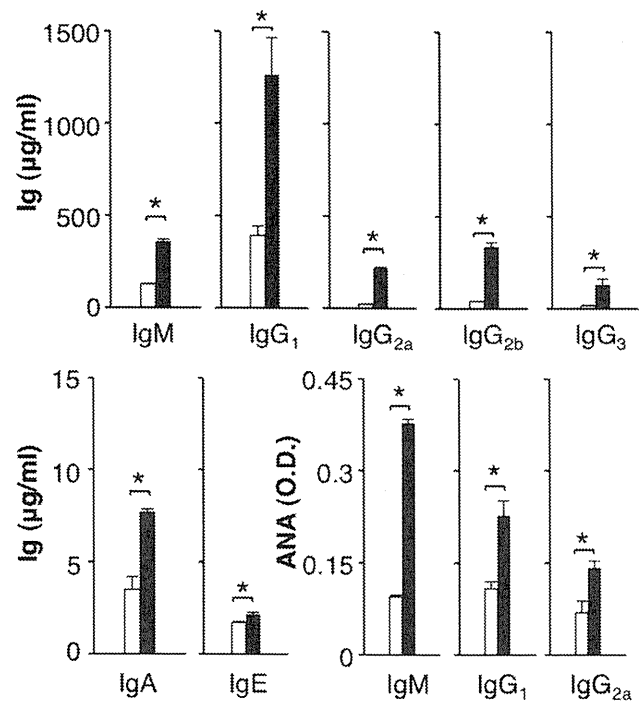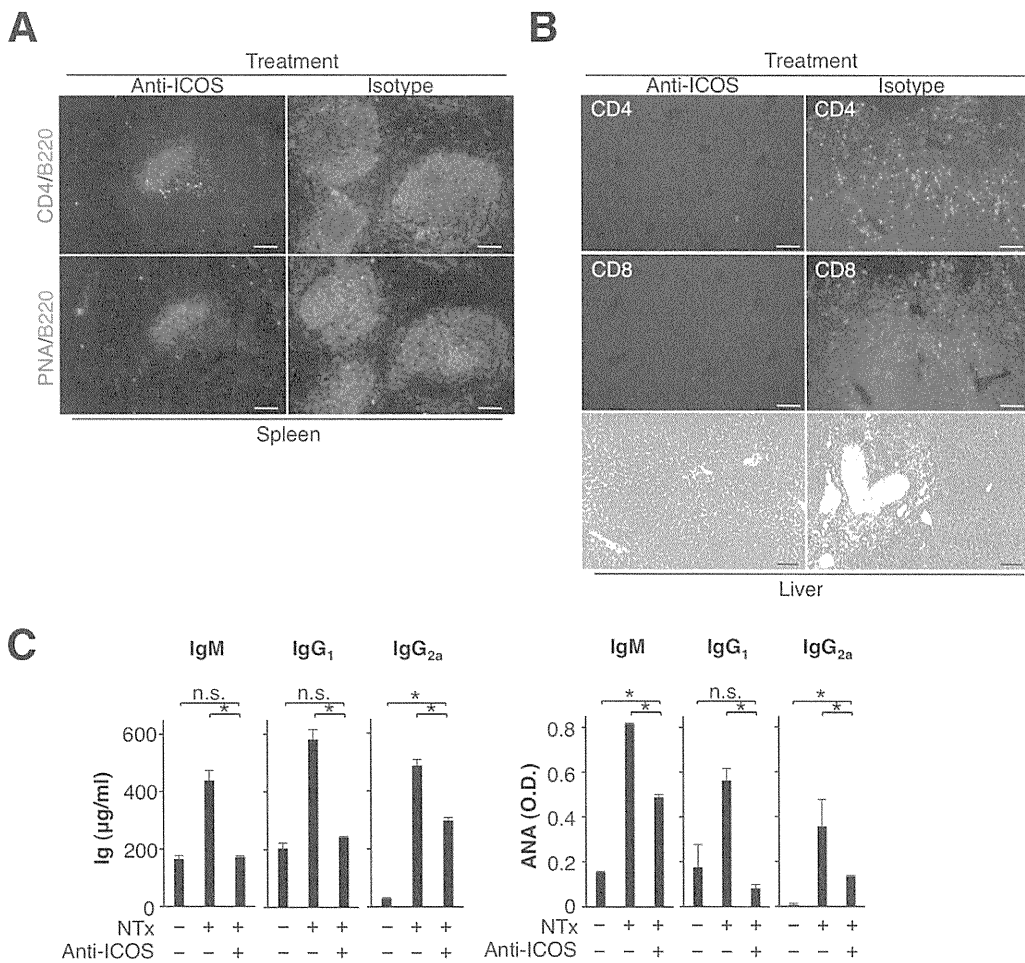

Supplementary Figure 3. Three-week-old NTx-PD-1$^{-/-}$ mice show hyper-γ-globulinemia and vast production of class-switched antinuclear antibodies (ANAs). The serum levels of total Ig subclasses and ANAs in IgM, IgG1, and IgG2a of 3-week-old PD-1$^{-/-}$ mice with (*solid columns*) or without (*open columns*) NTx determined by ELISA. *Bars* indicate the mean of each group, and *horizontal short bars* indicate the standard deviation. *$P < .05$.
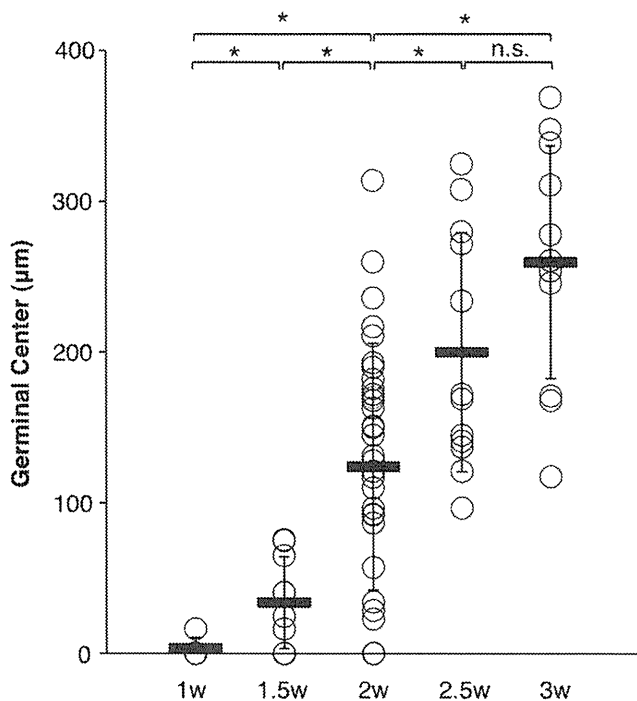

Supplementary Figure 2. The size of GCs is increased in the spleen of NTx-PD-1$^{-/-}$ mice from 1 to 3 weeks of age. Spleens from NTx-PD-1$^{-/-}$ mice at the indicated age in weeks were stained with FITC-conjugated PNA and biotin-labeled anti-B220 followed by Texas red-conjugated avidin. Each *open circle* represents a size of GC as measured in high-power fields. *Horizontal bars* indicate the mean size (diameter) of GCs in at least 3 sections. *Horizontal short bars* indicate the standard deviation. *$P < .05$.
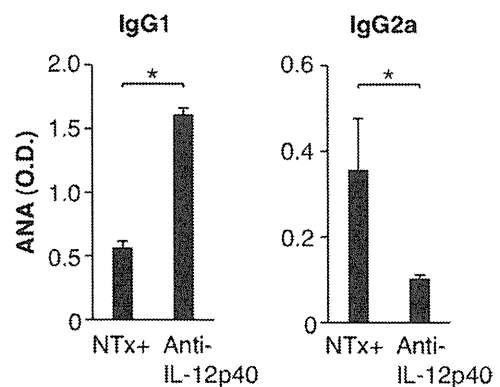
Supplementary Figure 4. Administration of anti–IL-12p40 induces increase of IgG1 and decrease of IgG2a classes of antinuclear antibodies (ANAs). NTx-PD-1$^{-/-}$ mice were injected intraperitoneally at 1 day after NTx and then once a week with anti–IL-12p40 (n = 5) Abs. After 4 injections, mice at 4 weeks of age were killed, and the serum levels of ANAs in IgG1 and IgG2a were determined by ELISA. *Bars* indicate the mean of NTx-PD-1$^{-/-}$ with or without administration of anti–IL-12p40, and *horizontal short bars* indicate the standard deviation. *$P < .05$.

Supplementary Figure 5. Administration of anti-ICOS suppresses not only T$_{FH}$-cell generation but also induction of fatal AIH, including hyper-γ-globulinemia and vast production of class-switched anti-nuclear antibodies (ANAs). (*A–C*) NTx-PD-1$^{-/-}$ mice were injected intraperitoneally at 1 day after NTx and then once a week with either anti-ICOS (n = 5) or isotype (n = 7) Abs. After 4 injections, mice at 4 weeks of age were killed and the spleens and livers harvested. Double immunostainings of the spleen. (*A*) The spleens from indicated mice were stained with FITC-conjugated anti-CD4 or PNA (*green*) and biotin-labeled anti-B220 followed by Texas red-conjugated avidin (*red*). (*B*) Stainings of the liver for hematoxylin and eosin (*HE*), CD4, and CD8. (*C*) The serum levels of total Ig subclasses and ANAs in IgM, IgG1, and IgG2a were determined by ELISA. *Bars* indicate the mean of each group, and *horizontal short bars* indicate the standard deviation. *P < .05. All *scale bars*, 100 μm.
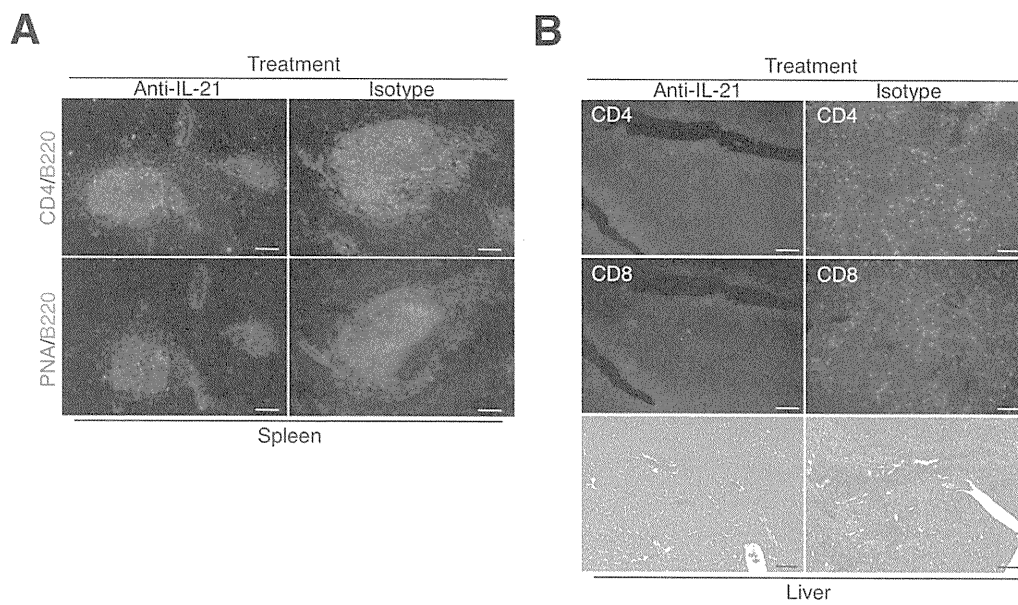
Supplementary Figure 6. Administration of anti–IL-21 suppresses not only T_{FH}-cell generation but also induction of fatal AIH. NTx-PD-1$^{-/-}$ mice were injected intraperitoneally at 1 day after NTx and then once a week with either anti–IL-21 (n = 5) or isotype (n = 5) Abs. After 4 injections, mice at 4 weeks of age were killed, and the spleens and livers were harvested. (A) Double immunostainings of the spleen. The spleens from indicated mice were stained with FITC-conjugated anti-CD4 or PNA (*green*) and biotin-labeled anti-B220 followed by Texas red-conjugated avidin (*red*). (B) Stainings of the liver for hematoxylin and eosin (*HE*), CD4, and CD8. All *scale bars*, 100 μm.

The incidence of deep vein thrombosis in Japanese patients undergoing endoscopic submucosal dissection

Masafumi Kusunoki, MD,[1] Kazumasa Miyake, MD, PhD,[1] Tomotaka Shindo, MD, PhD,[1]
Nobue Ueki, MD, PhD,[1] Tetsuro Kawagoe, MD, PhD,[1] Katya Gudis, PhD,[1] Seiji Futagami, MD, PhD,[1]
Taku Tsukui, MD, PhD,[1] Ikuyo Takagi, MD, PhD,[2] Junro Hosaka, MD, PhD,[3] Choitsu Sakamoto, MD, PhD[1]

Tokyo, Japan

Background: Endoscopic submucosal dissection (ESD) is more invasive than other common endoscopic procedures and may increase the risk for deep vein thrombosis (DVT)/pulmonary embolism. The incidence of DVT/pulmonary embolism after ESD has not been adequately studied.

Objective: To evaluate DVT incidence and disease-specific features of D-dimer levels in ESD patients.

Design: Prospective cohort study.

Setting: Single academic center.

Patients: This study involved 60 patients with superficial gastric neoplasms indicated for ESD.

Intervention: For all patients who underwent ESD, ultrasonography of the lower limbs was performed to detect DVT the day after ESD. D-dimer levels were measured 3 times: before ESD, immediately after ESD, and the day after ESD.

Main Outcome Measurements: DVT incidence after ESD.

Results: The DVT incidence was 10.0% (6/60). At all 3 time points, D-dimer measurements were higher in patients with DVT than in patients without DVT. According to receiver operating characteristic curve analysis, the resulting cut-off value of the D-dimer level the day after ESD was 1.9 μg/mL (sensitivity 83.3%; specificity 79.6%) for ESD patients, with superior association to pre-ESD or immediately after ESD. In univariate analyses, high D-dimer levels the day after ESD and the presence of comorbidities were significantly associated with DVT development.

Limitations: Single center and small number of patients.

Conclusion: ESD procedures have a moderate risk for venous thromboembolism. In patients undergoing ESD, D-dimer levels, especially on the day after ESD, may have specific features associated with DVT development. (Gastrointest Endosc 2011;74:798-804.)

Pulmonary thromboembolism (PTE) is a clinically serious condition in which a thrombus or other embolic process causes embolism in the pulmonary circuit. Overall, 90% of PTE results from deep vein thrombosis (DVT) involving veins of the lower limbs. Recently, PTE and DVT have been regarded as sequential conditions, and the general term venous thromboembolism (VTE) has been applied. VTE is both a social and a health care problem. Advanced age, malignant disease, inflammation, protracted bed rest, obesity, ischemic heart disease, and preg-

Current affiliations: Department of Internal Medicine, Division of Gastroenterology (1), Department of Internal Medicine (2), Division of Cardiology, Department of Radiology (3), Nippon Medical School, Tokyo, Japan.

Reprint requests: Kazumasa Miyake, MD, PhD, Department of Internal Medicine, Division of Gastroenterology, Nippon Medical School, 1-1-5 Sendagi, Bunkyo-ku, Tokyo 113-8603 Japan.

If you would like to chat with an author of this article, you may contact Dr Miyake at km366@nms.ac.jp.

nancy are among the known risk factors contributing to VTE.[1]

Endoscopic submucosal dissection (ESD) was developed to overcome the technical limitations of EMR.[2-4] ESD permits en bloc resection for larger lesions and has a higher rate of histologically complete resection (>80%) than conventional EMR.[5] However, ESD often necessitates that patients assume the same position for a prolonged period during and after the procedure, because of technical difficulties and frequent complications such as bleeding or perforation.[3,6] Therefore, the ESD procedure may be associated with a risk for VTE. It is thus important to confirm that the risk of thromboembolism is significant when ESD is performed and to predict the occurrence of DVT in order to prevent this clinically serious condition. However, the incidence of DVT among patients undergoing ESD has not previously been investigated.

The D-dimer is a marker of endogenous fibrinolysis and should therefore be detectable in patients with DVT. On the other hand, D-dimer levels vary depending on disease characteristics, sampling time points after surgery, and the amount of bleeding. Several studies have shown the D-dimer assay to be a sensitive but nonspecific marker of DVT.[7-9] However, disease-specific screening for DVT has received little attention.[10]

The present study aimed to evaluate DVT incidence and investigate the disease-specific features of D-dimer levels in patients undergoing ESD as a potential accurate marker of DVT.

METHODS

Study design and patient population

This prospective, cohort study was conducted from June 2007 to February 2009 at Nippon Medical School. We included consecutive patients aged at least 20 years with gastric neoplasms indicated for ESD. The lesions were judged by using magnified chromoendoscopy and pathology evaluation of biopsy specimens. The judgment was based on the expanded criteria for ESD. These criteria indicate an extremely low risk of lymph node metastasis, as reported by Gotoda et al.[11] The exclusion criteria were age >90 years; the presence of congenital and secondary coagulopathy, thrombophilia, malignancy other than gastric neoplasm, recent surgical procedures (within the preceding 12 months); pregnancy; use of estrogens; acute inflammatory disease, and body mass index (BMI) exceeding 30. Patients with preexisting coagulation disorders, as evidenced by DVT on ultrasonography of the lower limbs in the preoperative state, were also excluded. The following demographic characteristics were collected at screening before ESD: age, sex, BMI (18.5 kg/m^2 ≦ normal value range < 25.0 kg/m^2), comorbidities (chronic heart failure, chronic obstructive pulmonary disease, chronic renal disease, stroke), and use of anti-thrombotic drugs (warfarin, aspirin, ticlopidine, ethyl icosapentate, clopidogrel, and

Take-home Message

- This is the first prospective study to assess the incidence of deep vein thrombosis (DVT) after endoscopic submucosal dissection (ESD) for gastric neoplasia.
- ESD procedures have a moderate risk for thromboembolism. D-dimer levels, especially on the day after ESD, may have specific features in association with DVT development in ESD patients.

dipyridamole). When patients had taken anti-thrombotic drugs, therapy with these drugs was stopped from 5, 10, 14, 5, and 7 days before the ESD procedure, respectively, until at least the day after ESD. Patients who had been treated with warfarin were routinely treated with heparin when warfarin was discontinued, and heparin treatment was stopped 3 hours before and restarted 3 hours after ESD, as indicated in the guidelines.[12]

The protocol was approved by institutional review boards. Written, informed consent was obtained from all participants.

ESD

Gastric neoplasms were first identified and demarcated by using white-light endoscopy and chromoendoscopy with indigo carmine solution. ESD procedures were performed by using a flex-knife (KD-630L; Olympus, Tokyo, Japan), an insulation-tipped diathermy knife (IT knife; Olympus), and electrosurgical generators (VIO 300D; ERBE, Tubingen, Germany). Four operators (M.K., K.M., T.S., N.U.) carried out all ESD procedures in the present study. Patients were placed in the left lateral decubitus position on a pressure dispersion mattress and were sedated by intravenous injection of midazolam, flunitrazepam, and pentazocine. All patients were ordered to be at bed rest overnight after ESD, except for use of the lavatory, and none were given DVT prophylaxis.

Measurement of plasma D-dimer levels

Venous blood samples were collected at 3 time points: before ESD, immediately after ESD, and the day after ESD (18-24 hours after ESD). D-dimer levels were measured by the latex turbidimetric method (Nanopia D-dimer; Sekisui Medical, Tokyo, Japan: measurement range 0.5-60 μg/mL).

Diagnosis of DVT by ultrasonography of the lower limbs

We performed ultrasonography of the lower limbs for DVT detection at 2 time points: preoperatively and the day after ESD (24 hours after ESD). All examinations were performed by an experienced vascular technologist who used either an ATL Ultramark 9 or an ATL HDL 3000

computed sonography/color flow Doppler scanner (Advanced Technologies Laboratories, Bothell, Wash).

Statistical analysis

Depending on the type of baseline data, the results of comparisons between groups were analyzed by using a paired or unpaired t test for continuous variables. Continuous variables are expressed as mean ± SE. Crude associations for categorical data were evaluated by using a Fisher exact test or a chi-square test. One-way repeated-measures analysis of variance was performed on the plasma D-dimer data to identify interactions between time and groups or time-specific effects for each group. All P values were 2-tailed, and differences with values of $P <$ .05 were regarded as statistically significant.

Preoperative factors (age, sex, BMI, comorbidities, and use of anti-thrombotic drugs), and postoperative factors (operative time and D-dimer level) were included as potential risk factors for DVT in the univariate analysis. Odds ratios (OR) and 95% confidence intervals (CI) were calculated for risk factors. Statistical analysis was performed with StatView version 5.0 (SAS Institute, Cary, NC) or SPSS 11.0 for Windows (SPSS Inc, Chicago, Ill).

To identify the time of plasma D-dimer measurement indicating the highest diagnostic performance in terms of DVT development among 3 time points (before ESD, immediately after ESD, and the day after ESD), we used receiver operating characteristic (ROC) curve analysis. ROC curves for D-dimer levels were plotted by using Medcalc version 9 (Medcalc software, Mariakerke, Belgium). The area under the ROC curve (AUC) was calculated and then compared among the 3 time points. The time point with the largest AUC was defined as the most associated with DVT. Optimal cut-off points were determined on the basis of maximum values of the Youden index, calculated as [sensitivity + specificity − 1] and the minimum values of the square root of [$(1 - $ sensitivity$)^2 +$ $(1 - $ specificity$)^2$], which indicates minimum distance from the upper left corner to the point on the ROC curve.[13]

RESULTS

Patient characteristics

From June 2007 to February 2009, 71 patients with gastric neoplasms were enrolled in the study. Of these, 11 were excluded because of age exceeding 90 years (n = 1), incomplete follow-up (n = 5), detection of DVT on preoperative ultrasonography (n = 1), malignancy other than gastric neoplasms (n = 2), or recent surgical procedures (n = 2). Thus, 60 patients were studied and underwent ultrasonography postoperatively. The mean age of the patients was 71.2 years (range 49-88 years). Women accounted for 26.7% of patients. The mean BMI was 22.4

(range 16.5-28.8 kg/m^2). The mean operative time was 136.6 minutes (range 50-380 minutes).

Incidence of DVT after ESD

DVT was detected in 6 (10.0%; 95% CI, 2.3%-17.7%) of the 60 cases by ultrasonography the day after ESD. However, these patients with DVT were clinically asymptomatic.

Influence of ESD on plasma D-dimer levels in venous blood samples

After time-specific effects of D-dimer levels had been confirmed by 1-way repeated-measures analysis of variance in all patients ($P = $ .0009), D-dimer levels were compared among time points.

In all patients, D-dimer levels in venous blood samples increased significantly from 0.988 ± 0.123 μg/mL before ESD to 1.383 ± 0.257 μg/mL immediately after ESD and 1.997 ± 0.410 μg/mL the day after ESD ($P = $ .0411 or $P = $ .0026, respectively). Additionally, the D-dimer level the day after ESD was significantly higher than that immediately after ESD ($P = $ .0239 by paired t test). In patients with DVT, D-dimer levels immediately after ESD or the day after ESD tended to be elevated as compared with the before-ESD levels, although the difference in D-dimer levels between each time point was not statistically significant. In patients without DVT, there were no significant changes in D-dimer levels among any time points examined.

As shown in Figure 1, after interactions for times and groups of D-dimer levels had been statistically confirmed ($P = $ .001 by 1-way repeated-measures analysis of variance), the D-dimer levels were compared between patients with versus without DVT at each time point. The D-dimer levels were higher in patients with DVT than in those without DVT at all time points examined: before ESD (1.88 ± 0.746 μg/mL vs 0.89 ± 0.105 μg/mL; $P = $ .0147, unpaired t test), immediately after ESD (2.97 ± 1.722 μg/mL vs 1.2 ± 0.209 μg/mL; $P = $ .0368, unpaired t test), and the day after ESD (6.47 ± 3.44 μg/mL vs 1.5 ± 0.193 μg/mL; $P = $ .0002, unpaired t test) (Fig. 1).

Association with D-dimer levels and DVT development

The association with D-dimer levels and DVT development was assessed by using ROC curve analysis at 3 time points. As shown in Figures 2, 3, and 4, AUCs before ESD, immediately after ESD, and the day after ESD were 0.748 (95% CI, 0.620-0.852), 0.713 (95% CI, 0.582-0.822), and 0.843 (95% CI, 0.726-0.924), respectively.

Judging from the AUC values, the association with DVT development and D-dimer levels on the day after ESD was stronger than that before ESD or immediately after ESD. Thus, cut-off points showing optimal performance were